Deterministic Elastic-Plastic Modelling of Rough Surface Contact including Spectral Interpolation and Comparison to Theoretical Models

by

Bowen An

A thesis submitted to the Graduate Faculty of
Auburn University
in partial fulfillment of the
requirements for the Degree of
Master of Science

Auburn, Alabama
December 16, 2017

Keywords: Elastic-plastic, Rough Surface Contact, Finite Element Model

Approved by

Robert L. Jackson, Chair, Professor of Mechanical Engineering
Dan B. Marghitu, Professor of Mechanical Engineering
Jeffery C. Suhling, Department Chair of Mechanical Engineering

Abstract

Rough surfaces can be seen everywhere in our world, such as on table surfaces, roads, or cellphone screens. The interactions of rough surfaces are essential problems because they govern friction, wear, contact resistance and other phenomenon. A finite element elastic-plastic rough surface contact model is developed in this thesis. Multiple surface areas with different roughnesses are measured by an optical profilometer, which are selected from a S-22 Microfinish Comparator. A small square area with a side length of 31 micrometers is extracted from the measured rough surfaces. The area is populated with greater resolution by a novel method called spectral interpolation. The nodes covering the area are increased from 32 by 32 to 63 by 63 at the first interpolation, and to 125 by 125 at the second interpolation while the resolution decreases from one micrometer to 0.5 micrometer and 0.25 micrometer.

Visual inspection suggests that asperities of real surfaces are usually not sharp peaks but more rounded or curved. The spectral interpolation method allows for sharp peaks and intermediate points to be smoothed by adding additional nodes while keeping the surface spectrum constant. Therefore, the simulation results are presumed to be closer to cases of the real world. Then, the effects of different resolutions on the area-load relationship are studied by finite element simulation results and the results are compared to theoretical models. Additionally, the effects of the tangential modulus and different locations of the contact detection points used in the finite element method are also studied in the thesis. Different values of the tangential modulus (between 2% and 0% of the elastic modulus) result in significant changes of the area-load relationship.

Moreover, this work shows that using nodal points as contact detection points is a more reasonable choice than Gauss integration points.

Acknowledgments

I started working on this thesis from January 2017 under the supervision of my advisor, prof. Robert L. Jackson, the person I should be most grateful. He enlightened me about the thesis direction and gave me many useful suggestions when I met problems. I should thank Prof. Andres Carrano and his student Mr. Ali Khoshkhoo. They helped me to measure the data of many rough surfaces. I should thank Auburn university and the administer of Hopper. They offered me such a great environment and the facilities that needed for research. I should thank my groupmate, Mr. Xianzhang Wang, Mr. Yang Xu, Mrs. Xiaohan Zhang and Mr. Nolan Chu for their support and friendship. I should thank Prof. Dan B. Marghitu and Prof. Jeffery C. Suhling for serving on my thesis committee. I also should thank my parents because they always support me no matter where I am.

Table of Contents

List of Figures

List of Tables

List of Abbreviations

σ	Standard deviation
$\phi(z)$	Probability distribution function
σ_e	Equivalent roughness
σ_s	Standard deviation of asperity height
δ_i	Compressed height
α	Contact half-width
λ	Surface waviness period
ψ	Surface resistance to plastic deformation
η_i	Asperity density
β	Waviness amplitude
Δ, Δ_k	Amplitude of the sinusoidal surface
Δ_c	Critical amplitude
β_k	Equivalent 1D amplitude coefficient
λ_k	Wavelength of sinusoidal surfaces
n_i	*i* th number of layers
n_t	Total number of layers
A_c	Critical area
A_i	Contact area
A_r	Real contact area
A_n	Nominal contact area

$\overline{A}, \bar{A}_i$ Contact area of single asperity

a_i Contact radius

B_{max} Maximum ratio of amplitude to wavelength

d Separation

d_z Moving distance of node

E^* Effective elastic modulus

E_1, E_2 Elastic modulus of contact body 1 and 2

f Frequency

$\bar{F}_i$ Contact load of single asperity

F_c Critical load

F Total contact load

F^* Dimensionless total contact load

g Surface roughness amplitude

H Dimension between the top surface and the bottom surface

i Frequency level

K Kurtosis

k_x, k_y Frequency number

N_x, N_y Sample number

L Sampling length

m_n The nth Spectral moments

n Number of aspeirties

N Number of sampling points

$\bar{N}$ Total number of asperities

$\bar{p}$	Average pressure over the entire surface
$\bar{p}_c$	Critical average pressure over the nominal contact area
P_l	Elastic single asperity load
p^*	Sinusoidal pressure amplitude
p_m	Global mean pressure
p_p^*	Elastic-plastic average contact pressure
$\tilde{p}_{pp}$	Dimensionless average contact pressure
P	Total rough surface contact load
R	Asperity radius of curvature
R_a	Center-line average
R_q	Root mean square roughness
R_S	Relative radius of curvature
S_y	Yield stress
SK	Skewness
ν_1, ν_2	Poisson's ratio of contact body 1 and 2
W	Interference
w_c	Critical interference
w_l	Local contact load of a single asperity
z_0	Initial height of node
z	Surface height
z_{ave}	Average rough surface heigh

Chapter 1

Introduction

1.1 Surface Roughness

Rough surfaces may seem like irregular or uneven surfaces. However, all surfaces are rough to some degree. In other words, roughness is the natural state of surfaces. The surfaces of desks are rough. The screens of mobile phones are rough. Even the Earth, in a proper view from outer space, is rough. Therefore, interactions between rough surfaces often become essential problems. Actually, such kinds of interactions appear everywhere in our lives including in the fields of tribology, manufacturing and transportation.

Cases in the real world are more complicated than the model that we used in this thesis. Many environmental aspects may affect on the results of a simulation to differ in reality, such as temperature of the environment or contaminants adhered to surfaces. These effects are eliminated and only contact between a rough surface and a rigid flat plane is considered in this thesis.

The deviations of a real surface (in the normal direction) from its perfectly smooth form is called roughness. It is used to quantify how rough a surface is relative to a smooth surface. The surface is smoother with a small value of deviations and is rougher with a large value.

Roughness plays a significant role when there are interactions between two surfaces. Due to the importance of roughness, people devise various methods to measure the roughness, such as stylus profilometry and optical profilometry. A Nanovea ST400 optical profilometer was used in this thesis to measure the surface geometry.

1.2 Optical Profilometer

An optical profilometer (model ST400) manufactured by Nanovea was used to measure the surfaces (Fig. 1.1). It uses axial chromatism to measure surface height. A white light source with a high chromatic aberration passes through an objective lens. Light with different wavelengths will focus at different points because the objective lens has various refractive indices for various wavelengths of light. A monochromatic point is focused if samples (rough surfaces) are put at a proper range of distance. Then the topography of a rough surface is formed since only a specified wavelength is allowed to pass the spatial filter while all other wavelengths are blocked.

Figure 1.1 NANOVEA ST400 Optical Profilometer

1.3 Rough Surface Data

The surfaces of a S-22 Microfinish Comparator, as shown in Fig. 1.2, were measured by the optical profilometer ST400. The comparator consists of a total of 22 surface specimens. They are processed by six different methods, denoted by the following labels: L is for lapped, G is for ground, BL is for Blanchard ground, ST is for shape-turned, M is for milled and P is for profiled. The range of roughness of these specimens is from 2 to 500 micro-inches. The numbers following the labels such as 2, 4, 8, 125, 250, 500, are the average deviations from the mean level roughness and the unit of these numbers is micro-inches. The shape of the comparator is rectangular and it is a nickel duplicate of real surfaces. Three surfaces with different roughnesses, (4L, 8G and 16G) were selected for analysis. The measured size of each surface is 1023 um by 1023 um.

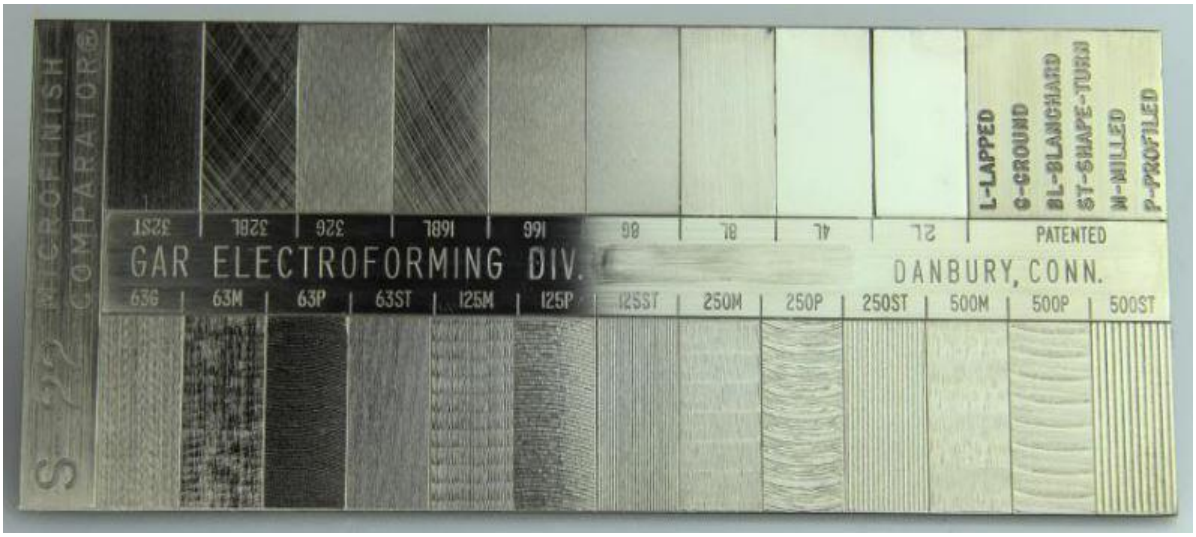

Figure 1.2 S-22 Microfinish Comparator

Fig. 1.3 shows the measured rough surface (1024 by 1024 nodes), which is one part of the 4L area. Fig. 1.4 shows the lower left corner of the measured surface with the size of 100 *um* by 100 *um*. Fig. 1.5 and 1.6 shows the measured surfaces from 8G and 16G, respectively. The scratches of 4L appear random in direction while marks on 8g and 16g are mostly in one direction.

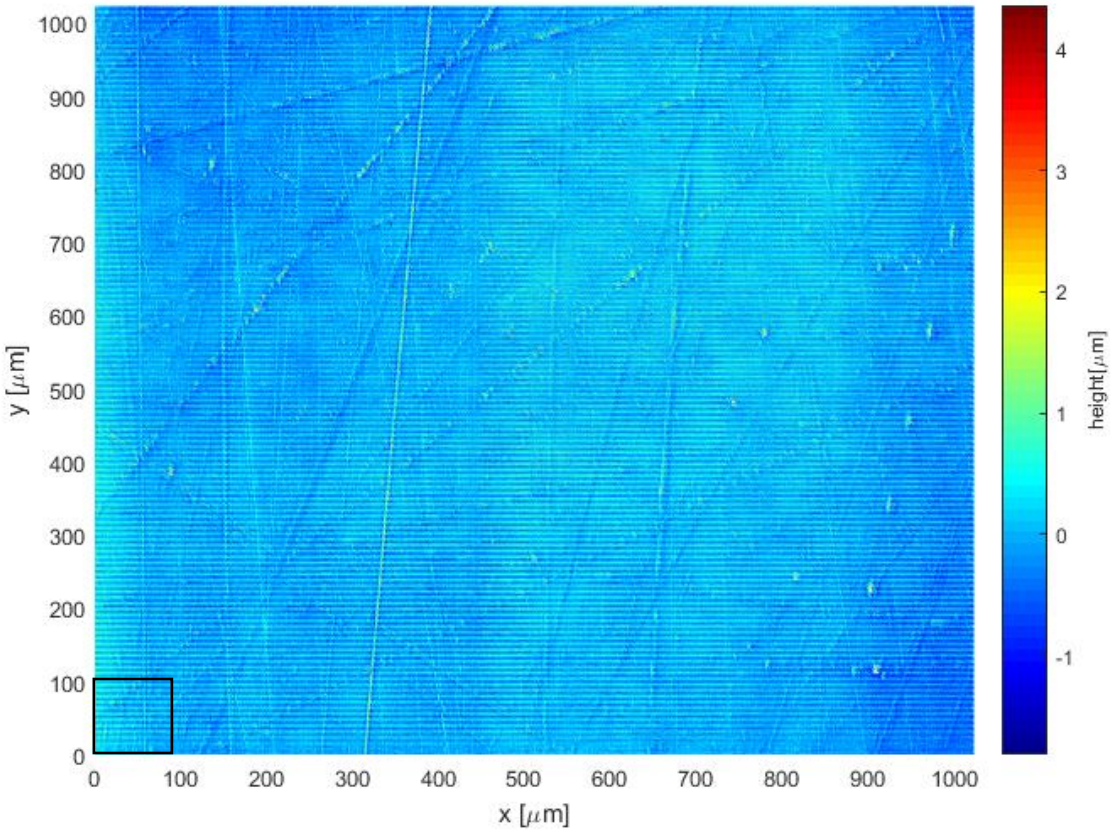

Figure 1.3 Measured surface from 4L

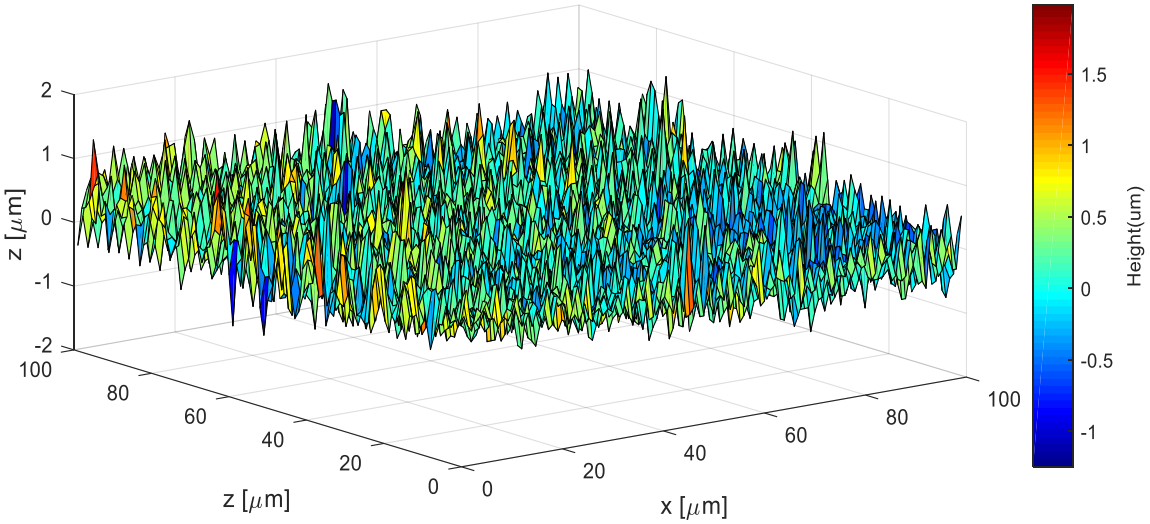

Figure 1.4 Lower left corner of the measured surface from 4L

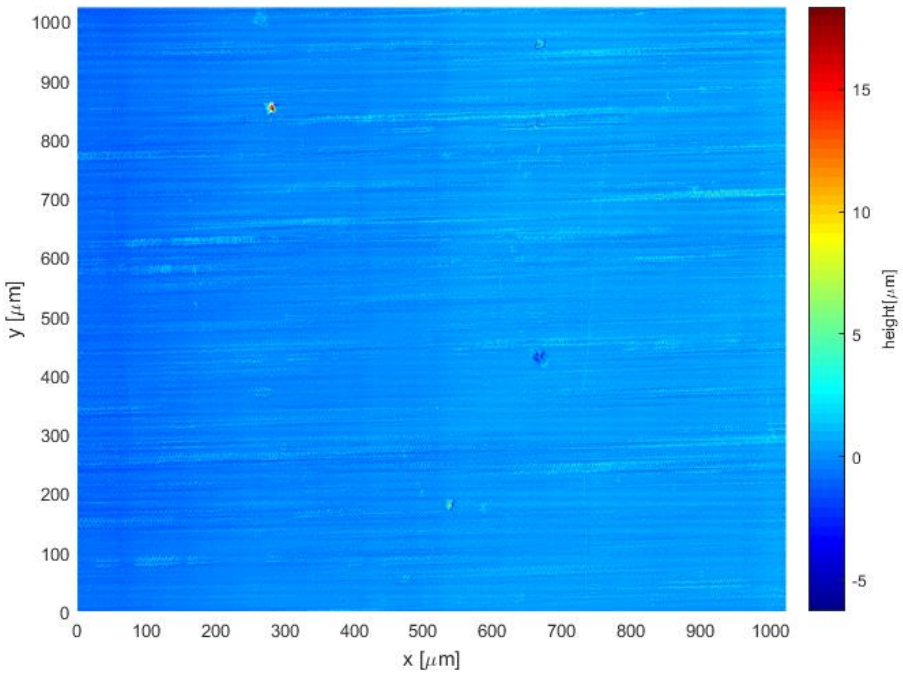

Figure 1.5 Measured surface from 8G

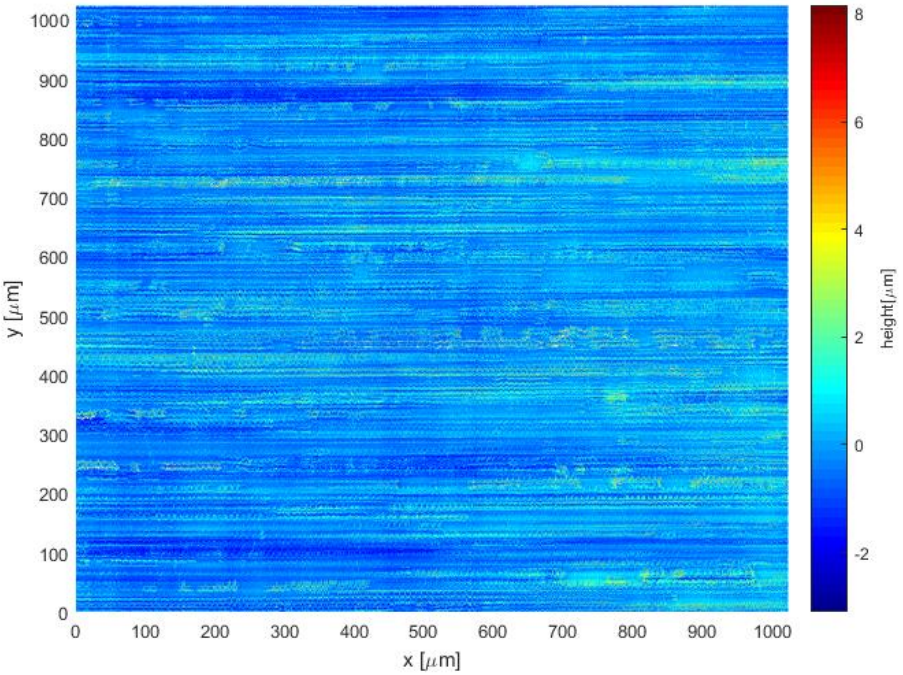

Figure 1.6 Measured surface from 16G

1.4 Statistical Description of Rough Surface

Since data of the measured rough surface was obtained, methods of describing roughness and rough surface geometries will be discussed in this section.

Fig. 1.7 presents a 2-D profile of the lower left corner of the measured rough surface. The peaks or rugged projections on the rough surface are called asperities. The tops of the asperities are referred to as summits. In other words, it is the highest point compared to the two adjacent points on the asperities.

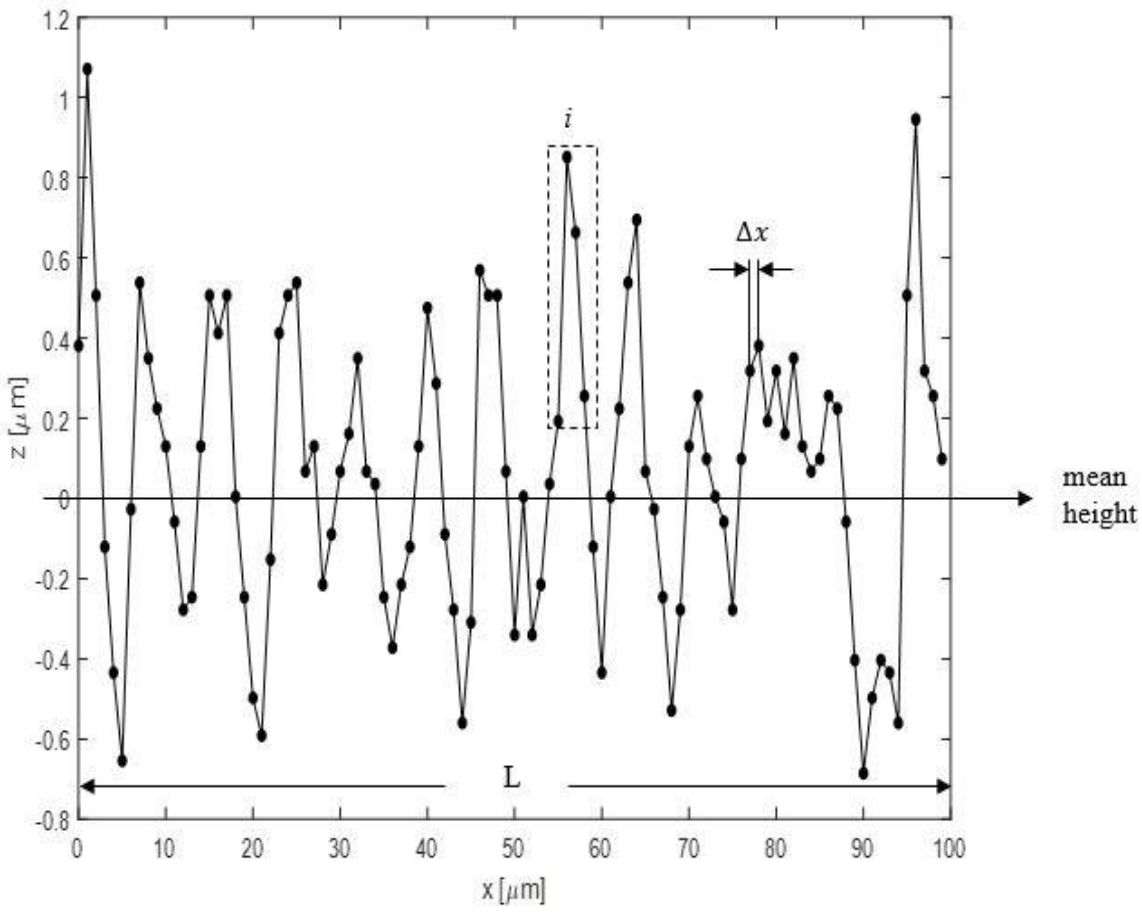

Figure 1.7 Sample 2-D asperity profile from the surface 4L

If roughness is ignored as two rough surfaces are in contact, the corresponding flat area when the two smooth surfaces come into contact is called the nominal contact area. Since real surfaces are never perfectly smooth because of roughness, the real contact area is a very small part of the nominal contact area. The ratio of the real contact area to nominal contact area is called the contact area ratio.

As shown in Fig. 1.5, Δx represents the interval between two consecutive nodes. The average height of the rough surface profile is called the mean height. In order to describe surface roughness effectively, the equation for the mean height or average [1] roughness is defined as:

$$R_a = \frac{1}{L}\int_0^L |z - z_{ave}|\, dx \tag{1.1}$$

where L is the sampling length and $z - z_{ave}$ is the height of rough surfaces above the mean height.

There is another measurement of surface roughness called R_q, which is the root mean square or standard deviation [1], σ, of the surface height from the mean surface height, Z_{ave}:

$$\sigma = R_q = \sqrt{\frac{1}{L}\int_0^L (z - z_{ave})^2\, dx} \tag{1.2}$$

R_q is more statistically meaningful because it is more sensitive to large deflections. The relationship between R_q and R_a is effected by the statistical nature of the surfaces. For Gaussian surfaces, the relationship [2] between R_a and R_q is defined as:

$$\frac{R_q}{R_a} = \sqrt{\frac{\pi}{2}} \approx 1.25 \tag{1.3}$$

Real surface heights are not measured continuously, therefore, the discrete form [4] of these two equations are used for calculating the roughness of measured surfaces:

$$R_a = \frac{1}{N}\sum_{i=1}^{N}|z_i| \tag{1.4}$$

$$R_q = \sqrt{\frac{1}{N}\sum_{i=1}^{N}{z_i}^2} \tag{1.5}$$

where *N* is the number of sampling points z_i is the zeroed and leveled height of the rough surface profile.

However, neither the average roughness nor the standard deviation can completely describe the shape of the rough surface profile statistically. Therefore, the moments of the distribution [3] are also used to quantify the shape of the rough surface profile.

m_n, the nth moment of a distribution is presented as:

$$m_n = \int_{-\infty}^{+\infty} z^n \phi(z)\, dz \tag{1.6}$$

where $\phi(z)$ is the probability distribution function.

The first moment, m_1, is the mean level of the surface profile and it is equal to zero because the level from which *z* is measured is usually used. The root of the second moment, m_2, is the standard deviation of the distribution or R_q:

$$m_2 = \int_{-\infty}^{+\infty} z^2 \phi(z)\, dz = \frac{1}{N}\sum_{i=1}^{N} {z_i}^2 = {R_q}^2 = \sigma^2 \tag{1.7}$$

The third moment is related to the skewness, *SK*, which describes the symmetry of the distribution. The skewness of a symmetrical distribution like a Gaussian distribution is equal to zero. Mathematically it is:

$$m_3 = \int_{-\infty}^{+\infty} z^3 \phi(z)\, dz \tag{1.8}$$

$$SK = \frac{m_3}{\sigma^3} = \frac{1}{\sigma^3}\int_{-\infty}^{+\infty} z^3 \phi(z)\, dz = \frac{1}{\sigma^3 N}\sum_{i=1}^{N} {z_i}^3 \tag{1.9}$$

The fourth moment is related to the kurtosis, *K*, which describe the sharpness of the peaks of the distribution (*K*=3 for a Gaussian surface). The distribution becomes flatter as the value of *K* increases. It is defined as:

$$m_4 = \int_{-\infty}^{+\infty} z^4 \phi(z)\, dz \tag{1.10}$$

$$K = \frac{m_4}{\sigma^4} = \frac{1}{\sigma^4}\int_{-\infty}^{+\infty} z^4 \phi(z)\, dz = \frac{1}{\sigma^4 N}\sum_{i=1}^{N} {z_i}^4 \tag{1.11}$$

In this chapter, the concept of roughness and rough surfaces are introduced and several methods for quantifying rough surfaces are given. Three rough surfaces with different roughness from a S-22 microfinish comparator are measured by a nanovea ST400 optical profilometer. Their geometries are presented in the Figs. 1.3, 1.5 and 1.6. The literature review and the purpose of this study will be detailed in the next chapter.

Chapter 2

Rough Surface Contact Review

Problems of rough surface contact have existed for as long as man has attempted to predict and control surface interactions. In order to understand the mechanisms behind the interactions of rough surfaces, many different methods have been developed for modeling rough surface contact. Tabor [4] in 1956 studied the pressure of plastic material indentation. He concluded that only one third of the mean contact pressure is effective in generating plastic flow. In the current thesis, we use 2.8 as the value of coefficient. By assuming all of the asperities are deforming plastically, the contact pressure can be assumed the hardness of indentation observed by Tabor. The hardness model is then simply the three times yield strength and is probably the simplest prediction of roughness contact area. This model is one of the earliest rough surface contact models. Otherwise, there are, basically, three different families of models: statistical models, multi-scale models, and deterministic models.

2.1 Statistical Rough Surface Contact Models

The statistical model is an important type of model in analyzing rough surface contact problems. In 1933, Abbott and Firestone [5] made the first attempt to describe the shape of rough surfaces by using the method of the probability distribution. They presented the bearing area curve (also called the Abbott-Firestone curve) by drawing lines parallel to the x-axis. The length of the fraction of the lines that lies within the surface profile increases as the height decreases, which describes how the bearing area curve relates to the distribution.

In 1966, Greenwood and Williamson [6] devised a contact model referred to as the GW model, which analyzed contacts between nominally flat but rough surfaces. Since the elastic stress is mainly decided by the relative profile of two rough surfaces, then the system can be replaced by a rigid flat surface and a deformable rough surface with the equivalent elastic modulus for plain strain and axisymmetry, E^*,

$$\frac{1}{E^*} = \frac{1-\nu_1^2}{E_1} + \frac{1-\nu_2^2}{E_2} \tag{2.1}$$

where ν_1, ν_2 and E_1, E_2 are the Poisson's ratios and the elastic modulus of the two contact bodies. The roughness of two surfaces can also be combined together. The profile of the deformable rough surface in contact with a flat surface is equivalent to the original relative profiles of two surfaces. The equivalent roughness, σ_e, is expressed as

$$\sigma_e = (\sigma_1{}^2 + \sigma_2{}^2)^{\frac{1}{2}} \tag{2.2}$$

σ_1 and σ_2 represent the root mean square roughness of two rough surfaces respectively. This method, in which a rigid flat surface is in contact with a deformable rough surface, was also used in the current thesis. The more general form is

$$m_n = (m_n)_1 + (m_n)_2 \tag{2.3}$$

where *m* represents the moment, which is introduced in chapter one.

Greenwood and Williamson adopted the Gaussian distribution to describe the probability of asperity height. The probability density function, $\Phi(z)$, for a Gaussian distribution is

$$\Phi(z) = \frac{1}{\sqrt{2\pi}\sigma_s} \exp\left(-\left(\frac{z}{2\sigma_s}\right)^2\right) \tag{2.4}$$

where z is the surface height and σ_s is the standard deviation of the asperity heights.

Assuming that summits of the asperities are spherical with the same radius of curvature, R_s, and that adhesion, asperity coalescing, shoulder to shoulder contact, and neighboring asperity interaction can be neglected, the number of asperities, n, whose heights z are larger than the separation, d, are given by

$$n = \bar{N} \int_d^\infty \Phi(z) dz \tag{2.5}$$

where $\bar{N}$ is the total number of asperities on the rough surface. For a single asperity with a height z_i, the height compressed by the rigid flat surface is

$$\delta_i = z_i - d \tag{2.6}$$

The relationship between the contact area A_i, which is a small circular patch in their case, and the radius a_i is

$$A_i = \pi {a_i}^2 \tag{2.7}$$

By adopting the spherical Hertzian contact theory, the relationship between a_i and δ_i is given by

$${a_i}^2 = \delta_i \times R_S \tag{2.8}$$

Therefore, the contact area, A_i, is

$$A_i = \pi R_S (z_i - d) \tag{2.9}$$

The real total contact area, A, for statistical rough surfaces in contact is then

$$A = N\pi R_S \int_d^{\infty} \Phi(z)(\mathrm{z} - \mathrm{d})dz \tag{2.10}$$

likewise, the elastic single asperity load, P_i, is

$$P_i = \frac{4}{3} E^* {R_S}^{\frac{1}{2}} {\delta_i}^{\frac{3}{2}} \tag{2.11}$$

and the total rough surface contact load P is

$$P = \frac{4}{3} N E^* {R_S}^{\frac{1}{2}} \int_d^{\infty} \Phi(z)(\mathrm{z} - \mathrm{d})^{\frac{3}{2}} dz \tag{2.12}$$

Several extended research works were conducted based on the GW model. Greenwood and Tripp [7] dealt with curved surfaces in 1967 and misaligned asperities [8] in 1971. Hisakado [9] took the non-uniform radii of curvature of asperities into account in his 1974 research. Onions and Archard [10] in 1972 adopted the joint probability density function, which was originally developed by Whitehouse and Archard [11] in 1970, for analyzing the relationship between the real contact area and the contact load. Bush et al. [12] in 1979 also studied the area-load relationship by anisotropic rough surfaces.

The majority of contact models after the GW model assumed a Gaussian distribution of asperities. However, Polycarpou and Etsion [13] in 1998 found that the simplified exponential distribution often used in the GW model is not perfect in every practical case. They replaced it with other exponential distributions for more accurate results. McCool [14] in 1992 presented a two parameter Weibull distribution which is able to explain skewness in the asperity height distribution. Chilamakuri and Bhushan [15] in 1998 developed non-Gaussian surfaces. They studied the effects of skewness and kurtosis with different values of the standard deviation σ and the correlation length β^* on contact areas and contact pressures. They observed that positive

skewness and kurtosis (4-7.5) leads to a minimum contact area surface. Kim et al. [16] in 2006 did similar research on three dimensional elastic plastic non-Gaussian rough surfaces generated by computer with specific skewness and kurtosis.

Many have used a geometric truncation to model fully plastic contact, but the origin of the model is not verified. It incorrectly assumes that when a flat is in contact with a deformable rough surface, the real contact area in their model is simply the truncation area of the original profile of the rough surface. Nayak [17] in 1973 used the random process model [18] that he presented in 1971 to analyze the plastic rough surface contact. The rough surface was modeled as an isotropic, Gaussian, random process. In his paper, the interaction of continuous surfaces was considered and the relation between the contact patch density and the normal pressure ratio was evaluated. Francis [19] in 1977 gave a probabilistic model between random rough surfaces. His previous empirical functions [20] were used to describe the entire deformation range from elastic to fully plastic.

Since the contact models above are either fully elastic or fully plastic but neglect the intermediate range, Chang, Etsion and Bogy (CEB) [21] presented an elastic-plastic model by applying the volume conservation theory for the range of moderately loaded contacts. Some basic assumptions of the GW model were adopted, such as isotropic asperities of the same radius, *R*, no lateral interaction between asperities, and no bulk deformation.

The contact area of a single asperity, $\overline{A}$, in the CEB model was expressed as

$$\overline{A} = \pi R w (2 - \frac{w_c}{w}) \tag{2.13}$$

where R is the asperity radius of curvature. ω is the interference and ω_c means the critical interference at the inception of plastic deformation. The lower limits of the equation are the

asperity-based model of elastic contact and the upper limits of the equation are the surface micro-geometry model of plastic contact.

Since the effects of asperity interactions in a lot of the above statistical models was neglected, Zhao and Chang [22] in 2001 presented a micro-contact model including such effects in elastic-plastic rough surface contact problems. Their analysis showed that asperity interactions put significant effects on aspects such as the mean surface separation or micro-contact load redistribution. They also derived an equation for the asperity deformation ω, which is defined as

$$\omega = z - d + 1.12\frac{\sqrt{w_l p_m}}{E^*} \tag{2.14}$$

d is the separation based on asperity heights. z is the height of a given asperity. ω_l is the local contact load of a single asperity. p_m is the global mean pressure over the nominal contact area.

Peng and Bhushan [23] in 2002 presented a 3D numerical model based on the variational principle for analyzing the sliding contact behavior of layered elastic-plastic solids with rough surfaces. They predicted the contact statistics and evaluated its effects on friction, stiction and wear problems. They found that a stiffer layer can be used to reduce the adhesive friction by decreasing real contact area and wear-particle formation. They also found that a more compliant layer can bring higher friction or wear-particle formation by increasing the real contact area.

In 2003, Kogut and Etsion [24] presented an improved statistical elastic-plastic model for rough surface contact problems based on finite element results. Their model predicted several contact parameters such as separation, real contact area and real contact pressure by applying a finite element analysis of an elastic-plastic single asperity contact. They made a comparison with the original CEB model of 1987, which gave the same results under the condition of the pure elastic contact, whereas quite different results occur if the value of plasticity index is larger than one.

They reported several findings: First, rough surface contacts are largely affected by the plasticity index, ψ. If ψ is smaller than 0.6, it is the pure elastic contact problem. If ψ equals 1.4, the real contact area is starting to transform from the purely elastic to the elastic-plastic problem. If ψ is larger than 8, the contact problem is nearly purely plastic. Second, according to their models, the contact load does not affect the mean real contact pressure significantly. Then, the contact load was connected to the real contact area by an 'elastic-plastic hardness', which is in the form of $0.4^{\frac{1}{\psi}}H$.

In 2005, Jackson and Green [25] devised an elasto-plastic contact model between two rough surfaces. Their previous finite element results [26] of a spherical asperity contact were used in this paper to study the relationship between contact force, contact area and the separation of surfaces. Then, they compared the results with other models, such as the GW model [6], KE model [24] and CEB model [21]. They found that the KE model was incomplete on a single asperity scale and that the CEB model was inaccurate at some surface separations. They also found that the statistical models might not be effective at all conditions and that they are only valid for relatively low loads. This is also the reason that the statistical models are not compared to the FEM results of the current thesis.

2.2 Multiscale Rough Surface Contact Models

In 1957, Archard [27] developed a multiscale elastic rough surface contact model. This might be the first model to take the multiscale nature of rough surfaces into account. The structure used in his model was described as 'protuberances on protuberances', which means smaller protuberances are uniformly layered upon the top of larger protuberances. The protuberances were asperities that were modelled as spheres. Archard found a linear relationship between the real

contact area and the contact load, which theoretically explained the Amontons's Law- friction is directly proportional to normal load. However, his rough surface structure is too unrealistic to be used in practice.

Majumdar and Bhushan [28] developed a well-known contact model that is based on fractal roughness parameters in 1991. Their paper suggested that surfaces are structurally fractal, thus, the statistical parameters are scale-dependent. They used a geometric truncation between a fractal surface and a flat to calculate contact area and spot size. They also presented that the fractal roughness parameters significantly influenced the relation between the contact load and the real contact area. The dimensionless total contact load is given as

$$F^* = \frac{4\sqrt{\pi}}{3} G^{*(D-1)} g_1(D) A_r^{*\frac{D}{2}} \left[\left(\frac{(2-D)A_r^*}{D} \right)^{(3-2D)/2} - a_c^{*\frac{(3-2D)}{2}} \right] + K\phi g_2(D) A_r^{*\frac{D}{2}} a_c^{*\frac{(2-D)}{2}} \tag{2.15}$$

where

$$g_1(D) = \frac{D}{3-2D}\left(\frac{2-D}{D}\right)^{D/2};\ g_2(D) = \left(\frac{D}{2-D}\right)^{(2-D)/2} \tag{2.16}$$

$$A_r^* = \frac{A_r}{A_a};\ a_c^* = \frac{a_c}{A_a} \tag{2.17}$$

G and *D* in the Eq. 2.14 are the fractal roughness parameter and fractal dimension of a surface profile, respectively. They can be obtained from the W-M function's power spectrum:

$$S(w) = \frac{G^{2(D-1)}}{2ln\gamma} \frac{1}{\omega^{(5-2D)}} \tag{2.18}$$

where $S(w)$ is the power spectrum and ω represents the frequency.

In 1999, Ciavarella et al. [29] considered a linear elastic contact problem between an elastic half-plane and a rigid rough surface based on a Weierstrass series. This model followed the framework proposed by Archard. The partial contact solution of sinusoidal surfaces found by Westergaard [30] was used to derive the distribution of contact pressure at different scales. They found that the contact area decreases progressively as the scale value becomes larger.

In 2005, Gao et al. [31] studied the elastic-plastic contact of a two dimensional sinusoidal surface. They derived two equations for describing the behavior of the contact. The first one α, the extent of contact, was defined as

$$\alpha = a/\lambda \tag{2.19}$$

where a means the contact half-width and λ is the surface waviness period. The second one, ψ, the surface resistance to plastic deformation, was expressed as

$$\psi = gE^*/\lambda S_y \tag{2.20}$$

where E^* is the equivalent elastic modulus, S_y is the yield stress of the substrate and g is the surface roughness amplitude.

Jackson and Streator [32] in 2006 came up with a multiscale model for rough surface contact problems. They adopted the idea of 'protuberances on protuberances' which was created by Archard [27] by assuming that smaller asperities (higher frequency asperities) are uniformly layered upon the top of larger asperities (lower frequency asperities) and the contact area of a given frequency level cannot be larger than the contact area below it. They also assumed that each frequency level obtains the same total load and each asperity at a given frequency level shares the

same amount of load. Based on these assumptions, they created a relationship between the real contact area, A_r, and the nominal contact area, A_n, which was expressed as

$$A_r = \left(\prod_{i=1}^{i_{max}} \bar{A}_i \, \eta_i \right) A_n \tag{2.21}$$

and the contact load

$$\mathrm{F} = \bar{F}_i \eta_i A_{i-1} \tag{2.22}$$

where *i* represents a scale level and i_{max} denotes the smallest scale level used in the model. $\bar{A}_i$ and $\bar{F}_i$ are the real contact area and the contact force of a single asperity at a given frequency level. η_i is the areal asperity density at that frequency level, which was defined as

$$\eta_i = 2{f_i}^2 \tag{2.23}$$

assuming that $i_{max} = 1$, which means there is only one frequency level, then the real contact area A_r was expressed as

$$A_r = \bar{A}_1 \eta_1 A_n \tag{2.24}$$

where $\eta_1 A_n$ is the number of asperities at level one and $\bar{A}_1$ is the real contact area of a single asperity at this level. Therefore, their product can obtain the real contact area of this scale level.

If $i_{max} = 2$, then

$$A_r = \bar{A}_2 \eta_2 \bar{A}_1 \eta_1 A_n \tag{2.25}$$

the real contact area of scale level one $\bar{A}_1 \eta_1 A_n$ times the areal asperity density of scale level two η_2 gives the number of asperities at scale level two. Then the real contact area of scale level two

can be obtained by multiplying the real contact area of a single asperity at scale level two. This process continues by including additional scales until the smallest scale level is included in order to obtain the real contact area between rough surfaces.

In order to relate the real contact area to the contact load, the solution to the contact problem between a sinusoidal surface and a flat was employed by Jackson and Streator [32]. Johnson, Greenwood and Higginson [33] analyzed the three-dimensional waviness case and gave the equations relating area to pressure. They defined $\bar{p}$ as the average pressure over the entire surface. p^*, the sinusoidal pressure amplitude during complete contact, was defined as

$$p^* = \sqrt{2}\pi E^* \beta f \tag{2.26}$$

where E^* is the equivalent elastic modulus, β is the amplitude of waviness and f is the frequency. If $\bar{p} \geq p^*$, the complete contact is reached so there is no gap between surfaces, which in the contact of a multiscale model means the real contact area of the given frequency level is equal to the real contact area below it.

if $\bar{p} \ll p^*$, then

$$(\bar{A}_{JGH})_1 = \frac{\pi}{f^2}\left[\frac{3}{8\pi}\frac{\bar{p}}{p^*}\right]^{\frac{2}{3}} \tag{2.27}$$

if $\bar{p} \sim p^*$, then

$$(\bar{A}_{JGH})_2 = \frac{1}{f^2}\left(1 - \frac{3}{2\pi}\left[1 - \frac{\bar{p}}{p^*}\right]\right) \tag{2.28}$$

since the general analytical solution is not available, Jackson and Streator gave an equation, which was based on the experimental data offered by Johnson [33], to connect the two cases above.

For $\frac{\bar{p}}{p^*} < 0.8$:

$$\bar{A} = \left(\bar{A}_{JGH}\right)_1 \left(1 - \left[\frac{\bar{p}}{p^*}\right]^{1.51}\right) + \left(\bar{A}_{JGH}\right)_2 \left(\frac{\bar{p}}{p^*}\right)^{1.04} \tag{2.29}$$

For $\frac{\bar{p}}{p^*} \geq 0.8$:

$$\bar{A} = (\bar{A}_{JGH})_2 \tag{2.30}$$

Wilson, Angadi and Jackson [34] in 2009 presented an elastic-plastic multi-scale model for rough surface contact problems. This model was developed upon the previous elastic multi-scale model, so the assumptions of the elastic model were still employed. They adopted some equations from the FEM results by Krithivasan and Jackson [35], Jackson, et al. [36], Manners [37] and Johnson et al. [33] to predict the area-load relation during the elastic-plastic condition.

First, in order to determine where the plastic deformation begins, they gave the equations of the critical load, F_c, the critical area, A_c, and the critical average pressure over the nominal area $\bar{p}_c$:

$$F_c = \frac{1}{6\pi}\left(\frac{1}{\Delta f^2 E^*}\right)^2 \left(\frac{C}{2}\sigma_y\right)^3 \tag{2.31}$$

$$A_c = \frac{2}{\pi}\left(\frac{CS_y}{8\Delta f^2 E^*}\right)^2 \tag{2.32}$$

$$\bar{p}_c = \frac{1}{24\pi}\frac{(CS_y)^3}{(\Delta f^2 E^*)^2} \tag{2.33}$$

where $C = 1.295\exp(0.736\upsilon)$, υ is Poisson's ratio, f is frequency, Δ is the amplitude of the sinusoidal surface, S_y is the yield strength and E^* is the equivalent elastic modulus.

As discussed above, Johnson, Greenwood and Higginson [33] gave the equations to the area-pressure relationship for elastic sinusoidal contact. The equation $(\bar{A}_{JGH})_1$ was replaced to evaluate the plastic deformation by [34]

$$A_p = 2(A_c)^{\frac{1}{1+d}}\left(\frac{3\bar{p}}{4Cs_y f^2}\right)^{\frac{d}{1+d}} \tag{2.34}$$

where d is

$$d = 3.8\left(\frac{E'}{s_y}\Delta f\right)^{0.11} \tag{2.35}$$

the complete average contact pressure at elastic-plastic deformation p_p^* is defined as [34]

$$\frac{p_p^*}{p^*} = 0.992\left[\left\{\left(\frac{\Delta}{\Delta_c}\right)^{\left(\frac{10}{3}\left(\frac{\Delta}{\Delta_c}\right)^{-0.39}+\frac{9}{4}\nu^4+0.64\right)}\right\}^{-1}\right] \tag{2.36}$$

and the critical amplitude Δ_c is [34]

$$\Delta_c = \frac{\sqrt{2}s_y}{\pi E^* f\left[3e^{-2/3(\nu+1)} + 2\left(\frac{1-2\nu}{1-\nu}\right)\right]} \tag{2.37}$$

and the complete average contact pressure at elastic deformation p^* is the same as Eq. 2.21

Therefore, the equation of the contact area of an elastic-plastic sinusoidal asperity at a given frequency level is defined as [34]

$$\bar{A}_i = (A_p)\left(1 - \left[\frac{\bar{p}}{p_p^*}\right]^{1.51}\right) + (\bar{A}_{JGH})_2\left(\frac{\bar{p}}{p_p^*}\right)^{1.04} \tag{2.38}$$

Combining Eqs. (2.21-2.38) together, Jackson and Streator [32] were able to predict the real contact area as a function of the contact load.

Despite the results from the elastic-plastic multi-scale model being in good agreement with other models, the computational complexity can be cumbersome. Jackson [38] in 2010 developed a simplified version of the elastic-plastic multi-scale model. The asymptotic solutions of the 3D elastic sinusoidal contact and the equations from Jackson et al. were adopted. Then, these equations were substituted into the area-load ($A_r - F$) relationship, which is expressed as

$$A_r = \frac{F}{p_p^*} \tag{2.39}$$

because of the multi-scale nature of rough surfaces, the required pressure to flatten all asperities was defined as

$$p^* = \max[p_i^*] = p^*(B_{max}) \tag{2.40}$$

where *i*, same as before, indicates the scale level. Therefore, the simplified version was expressed as [38]

$$(A_r)_{elastic/plastic} = \frac{F}{\sqrt{2}\pi E' \left(\frac{\Delta}{\lambda}\right)_{max} \cdot 0.992^{\left[\left\{\left(\frac{\Delta_{max}}{\Delta_c}\right)\left(\frac{10}{3}\left(\frac{\Delta_{max}}{\Delta_c}\right)^{-0.39} + \frac{9}{4}v^4 + 0.64\right)\right\}-1\right]}} \tag{2.41}$$

where Δ_{max} is from the maximum ratio of the amplitude to wavelength of the entire surface spectrum. It can be found form a reduced 1-D spectrum calculated from a 2-D spectrum by the methodology that Streator and Rostami [39] used in their paper:

$$\Delta_k = \left[\sqrt{\sum_{k_y-1}^{N_y-1} \left| F(k, k_y) \right|^2} + \sqrt{\sum_{k_x-1}^{N_x-1} |F(k_x, k)|^2} \right] \tag{2.42}$$

$$B_{max} = \left(\frac{\Delta_k}{\lambda_k} \right)_{max} \tag{2.43}$$

where Δ_k is the equivalent 1-D amplitude coefficient, $F(k, k_y)$ and $F(k_x, k)$ are the 2-D Fourier coefficients, k_x and k_y are the frequency numbers, and N_x and N_y are the number of sample in the x and y directions, respectively. Δ_k and λ_k are the amplitude and the wavelength of the sinusoidal surfaces at each frequency level, *k*, respectively. Therefore, B_{max} can be found through Eq. 2.42 and 2.43.

2.3 Deterministic Rough Surface Contact Models

Deterministic models directly use all the surface data without compromise and their outcomes are exactly known. There are two kinds of rough surfaces applied in this section: computer-generated rough surfaces and measured, real rough surfaces.

Several methods can be used to conduct a deterministic model, such as the finite element method and the boundary element method. In this section, only the finite element method will be introduced.

Computer-generated surfaces were widely used in the deterministic modeling of rough surface contact. In 1992, Komvopoulos and Choi [40] used the finite element method on multi-asperity contacts. They focused on the plane-strain problem of an elastic half space in contact with a flat rigid surface having cylindrical asperities.

Tian and Bhushan [41] in 1996 came up with a new numerical method for the elastic and elastic-plastic contact of rough surfaces, which were generated by an exponential autocorrelation function. A variational principle was used in their work to reduce the time of computation. Therefore, three dimensional rough surface contact problems with finer meshes became possible.

Hyun et al. [42] in 2004 analyzed the non-adhesive and frictionless contact between an elastic body and a self-affine fractal surface by using the finite element method. The successive random midpoint algorithm was adopted to create the self-affine fractal surface, which was overlayed on a flat rigid substrate. They made several conclusions through the analysis, such as the relationship between the real contact area and the load is linear until the contact ratio reaches 5-10%. They also found that the load had no influence on the mean pressure in the contact areas. Pei, et al. [43] in 2005 also used a self-affine fractal surface to analyze similar elasto-plastic contact problems. They describe the dimensionless average contact pressure $\tilde{p}_{pp}$ as

$$\tilde{p}_{pp} = k_1 \left(\frac{S_y}{E^*}\right)^{\alpha_1} \tag{2.44}$$

where constants α_1 =0.75 and k_1 =0.5. They found that the area-load relationship rises linearly in all cases. This model will be compared to the results obtained in the current work.

The multi-asperity contact problem was also analyzed by Pasaribu and Schipper [44] in 2005. They presented a semi-deterministic contact model for analyzing contacts between a flat-layered surface and a multi-asperity rough surface. An array of spherical asperities with various radii and heights were used to model the rough surface in order to releave the assumption of an average asperity radius.

Megalingam and Mayuram [45] in 2009 developed a deterministic contact model by using the method of finite elements. Their model was based on Thompson's [46] method, which created

three-dimensional Gaussian rough surfaces by using the APDL (ANSYS Parametric Design Language). They released the assumptions used in the GW model, which are all asperities have same radius of curvatures. They also [47] presented a deterministic Gaussian rough surface contact model for analyzing the effects of various surface parameters in 2014. They generated a three-dimensional rough surface in ANSYS to analyze asperity interactions and the effects of elasto-plastic deformation. They showed that plastic deformation becomes more significant as the value of surface roughness becomes higher. Song et al. [48] in 2016 used a generated Gaussian rough surface to analyze elasto-plastic contact. They adopted the conventional mechanism-based strain gradient plasticity and compared the results with the predictions of the purely elastic condition and the J_2 plasticity analysis.

Real measured surfaces were also frequently used in the deterministic rough surface contact models. Liu et al. [49] in 2001 developed an elasto-plastic contact model to study the contact behavior of materials and geometry properties. The contact was analyzed between a real rough surface and a rigid flat plane. They analyzed the real contact area and the contact pressure of real rough surfaces under different deformation regimes such as elastic, elasto-plastic or elastic-perfectly plastic. Jamari et al. [50] in 2007 used a measured rough surface to study the contact behavior of the plastic contact. They did a theoretical and experimental analysis between a smooth sphere and a nominally flat rough surface.

Wang et al. [51] in 2010 presented a three-dimensional numerical model for analyzing elastic-plastic rough surface contact problems. The radial return method and J_2 flow theory were adopted by them to deal with the increment of plastic strain. Then, their elastic-plastic model was applied to a real ground engineering surface. Among these problems, they studied the

effects of surface roughness, the distribution of contact pressure, the location of the maximum residual von Mises stress value and the real contact area.

Jackson and Green [52] in 2011 made a comparison of the area-load relationship between several real surfaces with different roughness and a deterministic FFT-based contact model. They found that these theoretical models are basically in qualitative agreement and produce a nominally linear relationship while the deterministic model shows predictions that agree with some models but differ from others. Yastrebov et al. [53] in 2011 applied two approaches, the finite element method and a reduced model, for analyzing elastic rough surface contact problems. The rough surfaces were measured from eight matching samples. They studied the load-displacement relationship, the real contact area and the free volume by using the reduced model. The results of the FEA were used as a reference to calibrate the inputs of the reduced model. Additionally, they found that the CPU time of the second method is much less than the first method. Xu [54] in 2012 studied the elastic contact problems between a nominally flat rough surface and a rigid flat surface. He used two deterministic numerical methods to analyze the problem, the boundary element method and the finite element method. The comparison of the area-load relationship between two methods shows good agreement. Poulios and Kilt [55] in 2013 presented a finite element model for analyzing the rough surface contact problems. They studied the theoretical foundation of the model by making several calculation examples. In the first part, their model was compared to the GW theory to analyze the area-load relationship. In the second part, they took elastic-plastic properties into account in order to analyze the plastic deformation.

2.4 Summery

In the above section, we introduced many important models within the three families. In statistical contact models, Abbott and Firestone [5] in 1933 made the first attempt to describe the

shape of rough surfaces by using the bearing area curve. Greenwood and Williamson [6] in 1966 adopted the spherical hertzian contact theory for single asperity deformation and applied Gaussian distribution to describe the asperity height to predict the area-load relationship. Afterwards, many researches were conducted by releasing the assumptions used in the GW model, such as misaligned asperities [8] (Greenwood and Tripp 1971), non-uniform radii [9] (Hisakado 1974), anisotropic rough surfaces [12] (Bush et al. 1979), non-Gaussian rough surfaces (Chilamakuri and Bhushan [15] 1998 or Kim et al. [16] 2006).

Chang, Etsion and Bogy [21] (CEB) in 1987 presented an elastic-plastic contact model by considering the theory of volume conservation. They gave the equation of the contact area of a single asperity. Kogut and Etsion [24] in 2003 presented a statistical elastic-plastic rough surface contact model based on the finite element method. They compared their results with the CEB model. The results were in good agreement in purely elastic case and quite different if the plasticity index is larger than one. Jackson and Green [25] in 2005 presented an elasto-plastic contact model. Their results were compared with many previous models, such as the GW model [6], KE model [24] and CEB model [21]. According to the comparison, they proved that some of these statistical models are either incomplete or inaccurate when they are used to predict large deformations.

In multiscale contact models, Archard [27] in 1957 developed the first multiscale model as he described as ‘protuberances on protuberances’ structure. Majumdar and Bhushan [28] in 1991 presented a contact model that is based on fractal roughness parameters. Jackson and Streator [32] in 2006 presented an elastic multiscale model based on the structure of Archard. Their model predicted the area-load relationship and was compared to the GW model and the MB model. The trends between these three models are very similar while the JS model is not as sensitive to the sampling resolution. Wilson et al. [34] in 2009 devised an elastic-plastic multiscale model to

predict the area-load relationship. The results do not agree quantitatively with the statistical contact models in comparison. Jackson [38] in 2010 developed a simplified version of the multiscale model to predict the area-load relationship in order to reduce the complex computation of the previous elastic-plastic model. Many previous works, including a deterministic elastic contact simulation, were used to compare with the results of the simplified model and they are in good agreement.

In deterministic contact models, Tian and Bhushan [42] in 1996 applied a variational principle in a new numerical method to analyze the elastic-plastic rough surface contact problems. This method is able to reduce the time of computation significantly, thus finer meshes with a larger number of contact points become possible.

Hyun et al. [43] in 2004 studied the contact problems between self-affine surfaces. They found that the area-load relationship remains linear until the contact ratio reaches 5-10%. They also found that the contact load puts no effects on the mean pressure in the contact areas. Pei et al. [44] in 2005 analyze similar elasto-plastic contact problems. They gave the equations for the dimensionless average contact pressure and compared their results to previous works of elastic solids. They found that the area-load relationship rises linearly in all cases.

Megalingam and Mayuram presented a deterministic contact model based on Thompson's method in 2009 [45] and 2014 [46] respectively. Wang et al. [50] in 2010 developed a 3D model for elastic-plastic rough surface problems. The results were compared to the FEM results of three typical contacts and the comparison shows a good agreement. Jackson and Green [51] in 2011 compared the area-load relationship between several real surfaces with different roughness and a deterministic FFT-based contact model. They found that these theoretical models are basically in qualitative agreement and produce a nominally linear relationship while the deterministic model

is only in good agreement with some of the models. Xu [53] in 2012 analyzed the elastic rough surface contact problems. He used both the boundary element method and the finite element method in his research. The comparison of their results of the area-load relationship shows good agreement, however, he argued that the boundary element method is superior for modeling rough surface contact.

Chapter 3

Numerical Simulation

In this chapter, the method of spectral interpolation is introduced and the finite element modeling is described. An extracted area from the surface 4L is used to simulate rough surface contact in ANSYS. The process of simulation are described in detail including modeling, meshing and applying boundary conditions.

3.1 Data Processing

3.1.1 Preprocessing Data

Using a *ST*400 the 3D optical profilometer, the data of three rough surfaces with 1024 by 1024 nodes was obtained. First, a small part of the rough surface with 32 by 32 nodes was extracted from the 4L surface. This extracted portion of the surface is shown in Fig. 3.5. The mean height was subtracted and the surface was leveled by using the curve fitting function in MATLAB.

3.1.2 Spectral Interpolation

In previous works of deterministic elastic-plastic rough surface contact problems, researchers either used generated rough surfaces or measured rough surfaces in the simulations. In both kinds of rough surfaces, the shape between two consecutive nodes was assumed as linear. However, this thesis assumes a harmonic relationship instead of a linear relationship by using the method of spectral interpolation.

After a leveled and zeroed surface with a proper size is acquired, the spectral interpolation is the next step. First, a 2-D fast Fourier transform was used to transfer the data of the rough surface into

the frequency domain and then placed into the center of a zero array with the size of 64 by 64. This method is called zero padding, which is able to increase the length of the original data by adding zeros. The zeros represents higher frequencies that add no information to the surface. The process is shown in Fig 3.1 (from Z3 to Z4). Second, the inverse 2-D fast Fourier transform command was used to transfer the frequency domain back to the spatial domain. Then the mesh of the original surface was enlarged to either 63 by 63 and 125 by 125. Then, the surface with 63 by 63 nodes and 125 by125 nodes were obtained. Fig. 3.2 is a 2-D profile of the original surface. Figs. 3.3 and 3.4 are 2-D profiles of the interpolated surfaces compared with the original surface.

Since the nominal contact area remains unchanged, the interval between two consecutive nodes for 32 by 32, 63 by 63 and 125 by 125 decreases progressively from 1, to 0.5, and to 0.25 micrometers, respectively. Figure 3.5 is the three-dimensional profile of the original 32 by 32 surface. Figs. 3.6 and 3.7 are the interpolated three-dimensional profile with 63 by 63 nodes and 125 by 125 nodes, respectively. Figs. 3.5, 3.6 and 3.7 are from the same perspective. After interpolation, the maximum values and the minimum values changed slightly. However, the spectrum of all surfaces are exactly identical and the nominal contact area remains constant.

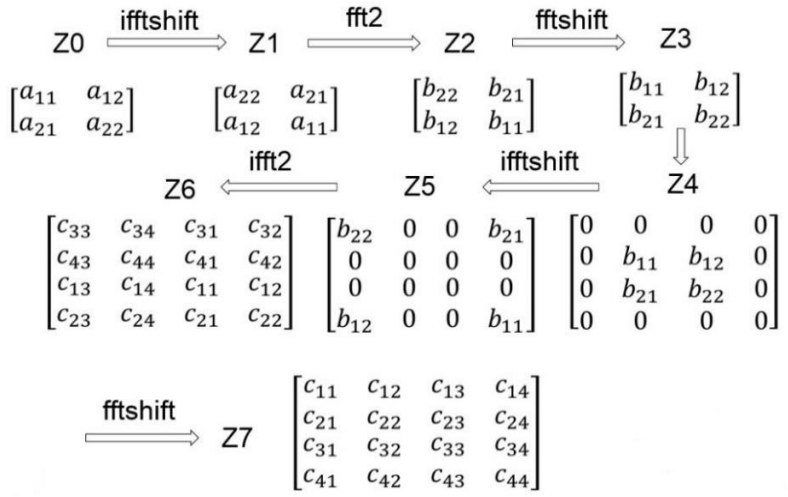

Figure 3.1 Principle of spectral interpolation

Additionally, several important details in the Fourier transformation in Matlab were noticed in conducting this study. Every single time before using the Fourier transformation, such as the fft*2* or ifft2 command in MATLAB, the zero frequency areas must be at the corners of the frequency domain matrix. This process can be done by using the MATLAB commands fftshift and ifftshift. The command fftshift moves the zero frequency component to the center of the array while the ifftshift command does the opposite.

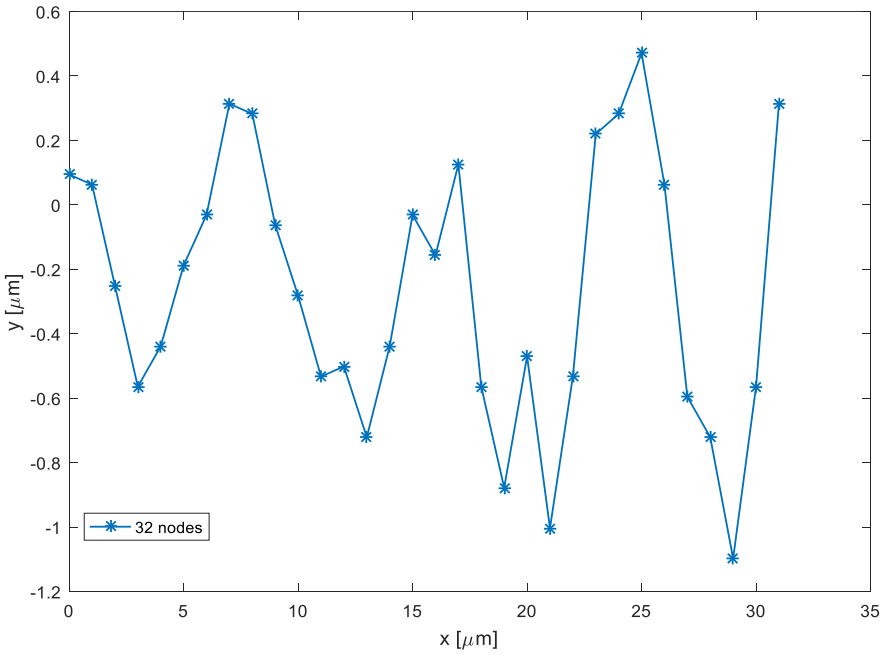

Figure 3.2 2-D profile of 32 by 32 nodes surface

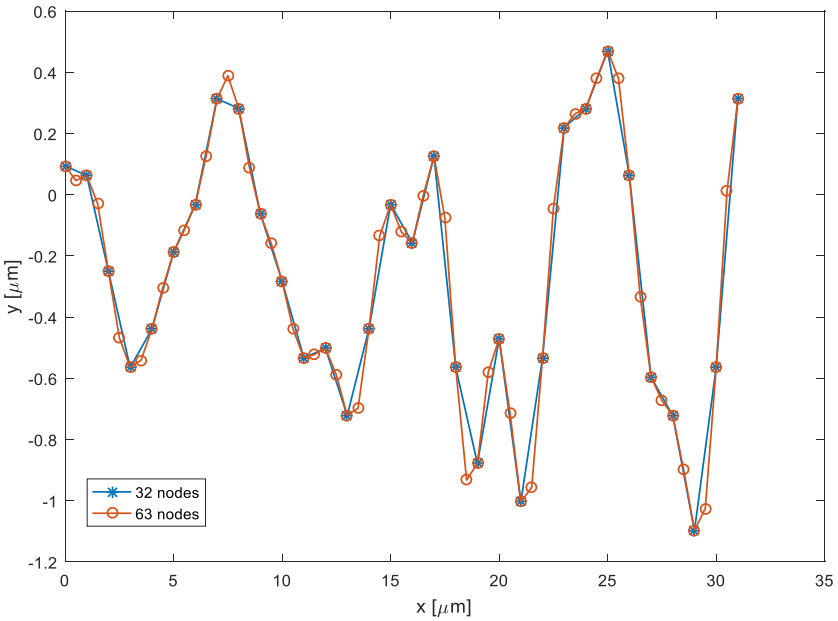

Figure 3.3 2-D profile of interpolated 63 by 63 nodes surface

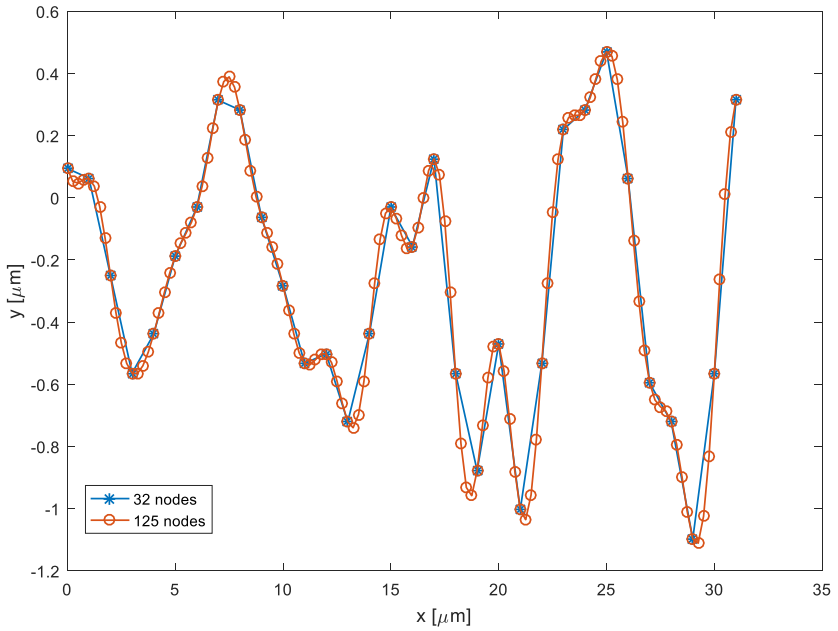

Figure 3.4 2-D profile of interpolated 125 by 125 nodes surface

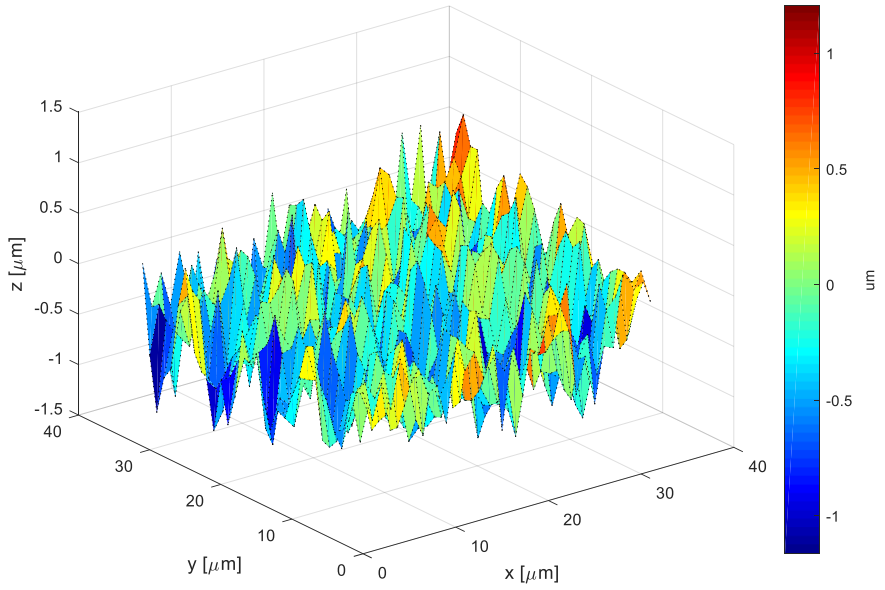

Figure 3.5 32 by 32 nodes rough surface

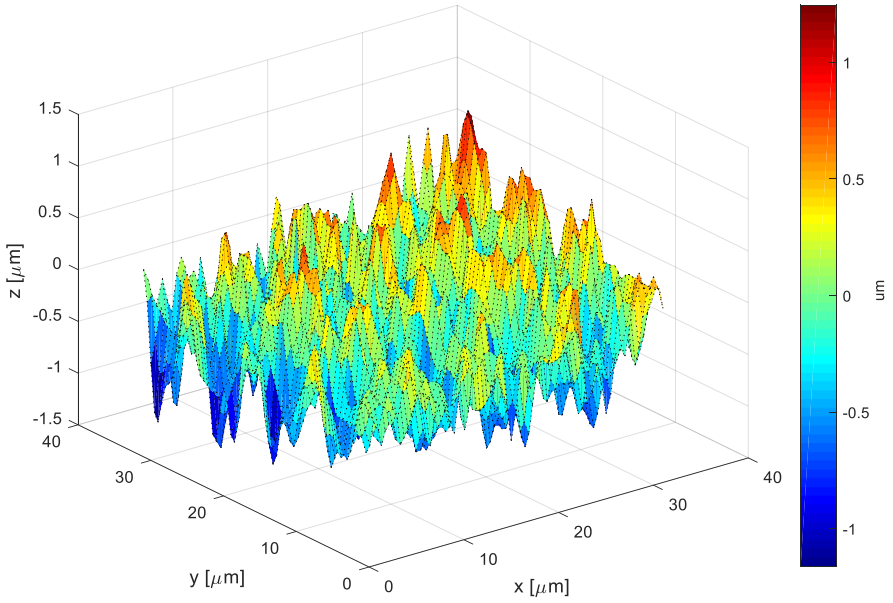

Figure 3.6 63 by 63 nodes rough surface

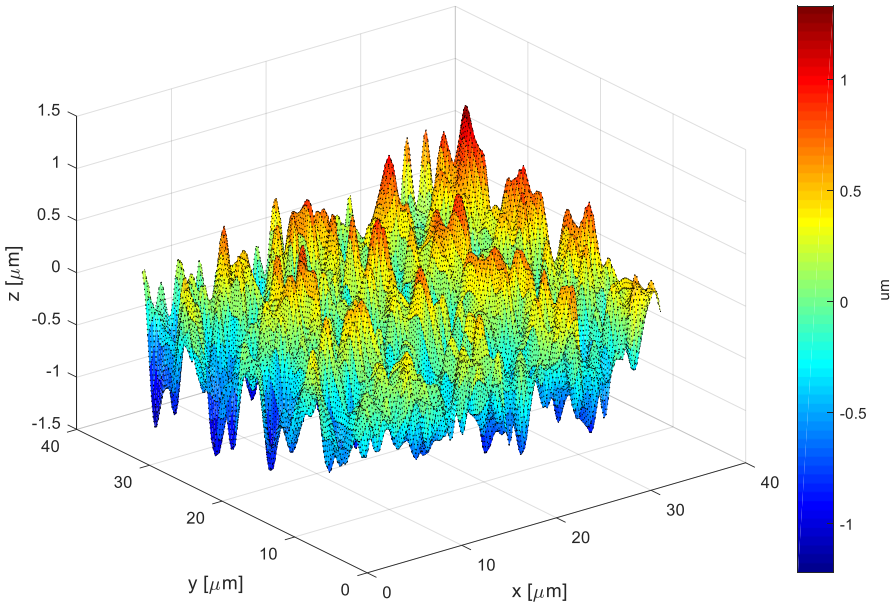

Figure 3.7 125 by 125 nodes rough surface

3.2 Finite Element Methodology

3.2.1 Introduction

The finite element method (FEM) was used in this work to analyze rough surface contact problems. In the method, the entire model is divided into many smaller parts named elements. Points that connect elements are called nodes and the arrangement of elements is called a mesh. Formulation of each finite element leads to an algebraic equation. The equation of each finite element are assembled into a larger system of equations. Then, the solution over the entire model is solved.

Finite element analysis (FEA) acts as a computational tool in the field of engineering. $ANSYS^{TM}$, a commercial finite element software, is able to simulate static, thermal, electrical, fluid and

structural problems. In the current thesis, a finite element model was created and studied by using $ANSYS^{TM}$ Parametric Design Language (APDL).

3.2.2 Element Selection

Solid 185, a 3-D 8-node homogeneous structural solid element, was used to mesh the geometry. Fig. 3.8 represents a solid element used in the model. Each node has three degrees of freedom in *x*, *y* and *z*. The elements possess capabilities of plasticity and large deflection.

TARGE170, a 3-D 4-node surface to surface target element, is used for target surfaces associated with the contact element CONTA173. A pilot node was set to define the degrees of freedom for the entire target surface.

CONTA173, a 3-D 4-Node Surface-to-Surface Contact Element, allows the model to consider normal contact between the target surface and a deformable surface. The contact algorithm used is the Augmented Lagrangian Method. The location of the contact detection point is on a node, which is normal to the target surface. Both the target element and the contact element were used for pair-based contact. They shared the same real constant set, which specified the various contact properties, such as stiffness.

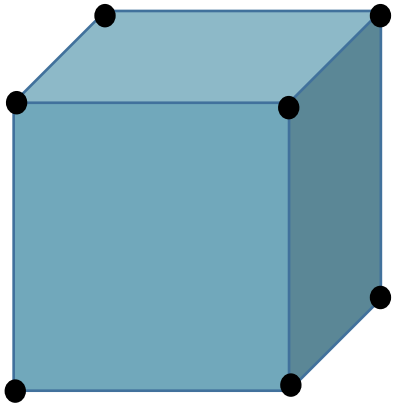

Figure3.8 A solid element

3.2.3 Material Properties

The material is being modeled as an elastic-plastic material with bilinear isotropic hardening. The elastic modulus is 200GPa, the Poisson's ratio is 0.3, the yield strength is 1GPa and the tangential modulus is 100MPa. Their relationship is described by the uniaxial stress-strain curve in Fig. 3.9. The slope of the line from the origin is the elastic modulus, E. The second slope, at stresses beyond the yield strength σ_0, is defined by the tangential modulus, E_T. The value of E_T cannot be larger than the elastic modulus. For the elastic perfectly-plastic case with no hardening, E_T equals zero.

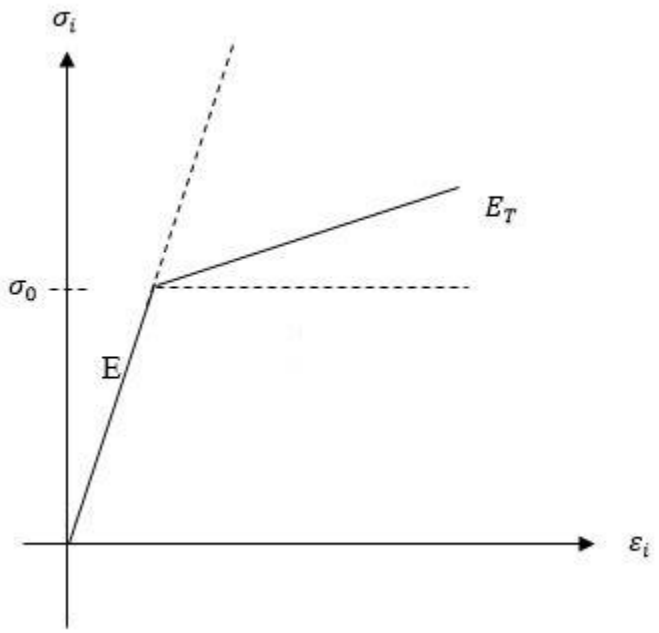

Figure 3.9 Stress-strain curve for bilinear isotropic hardening

The normal contact stiffness applied in the contact elements is a critical value because it affects many aspects, such as the amount of penetration between the surfaces. A large penetration will induce errors in the results because the contact condition is violated. The amount of penetration decreases as the value of contact stiffness rises, but a high value of contact stiffness will lead to

convergence difficulty. Therefore, the normal contact stiffness factor is varied according to the conditions of different cases. In this work, the penetration depths were checked to be small so that the contact condition is properly enforced.

3.2.4 Mesh Generation

3.2.4.1 Geometry

The model was made of two components-rough surface layers (Fig. 3.10) and a substrate (Fig. 3.11). Rough surface layers were used for moving nodes intermediately for creating the rough surface. The thickness of each layer is exactly the same and the number of layers is varied according to different surface details. Three layers were used for the case of 32 by 32 nodes and five layers were used for the cases of 63 by 63 and 125 by 125 nodes. The purpose of the substrate is to provide a volume for bearing the rough surface layers and the goal is for the case of a rough surface on a half-space to be effectively represented. The thickness of the substrate is also varied according to different surface details, such that the thickness is large enough so that the model effectively represents a half-space.

3.2.4.2 Meshing

The volume was meshed by the solid 185 element. Mapped meshing was used for the rough surface layers and free meshing was used for the base. The number of element divisions within the substrate decreases progressively from the base to the rough surface layers in order to reduce the total number of elements as well as to maintain mesh quality. Different ways of meshing were conducted to the volume in order to obtain mesh convergence, such as vsweep method or mapped mesh for the whole volume. Fig 3.12 is the meshed volume with the rough surface layers and base. Fig. 3.13 is the meshed volume with the target surface also shown. Figs 3.10-3.13 represent the

case of a 32 by 32 node surface. The mesh structure of the 63 by 63 case (Fig. 3.14) and 125 by 125 case (Fig.3.15) are very similar to the case of 32 by 32 but have slight adjustments according to their different geometries.

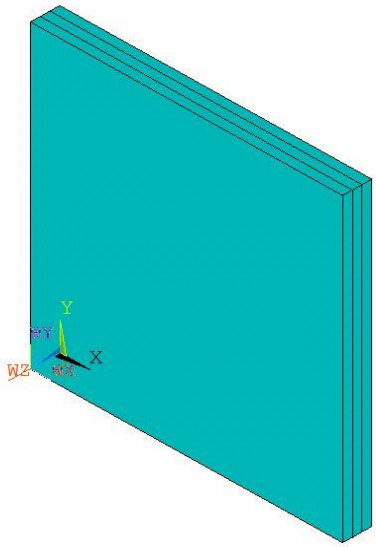

Figure 3.10 Rough surface layers

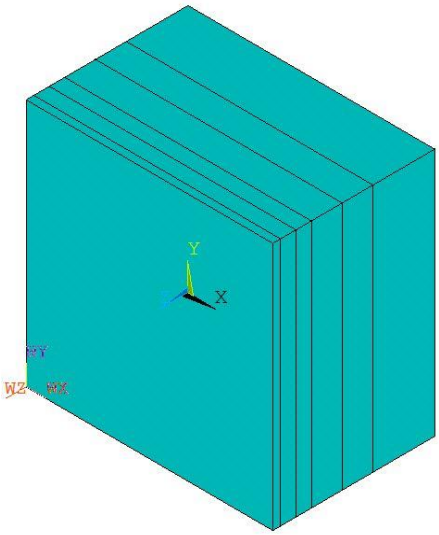

Figure 3.11 Substrate

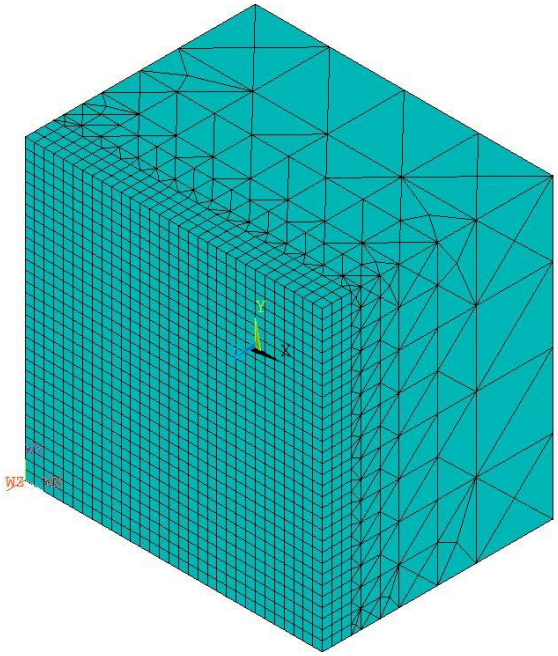

Figure 3.12 Meshed volume (32 by 32)

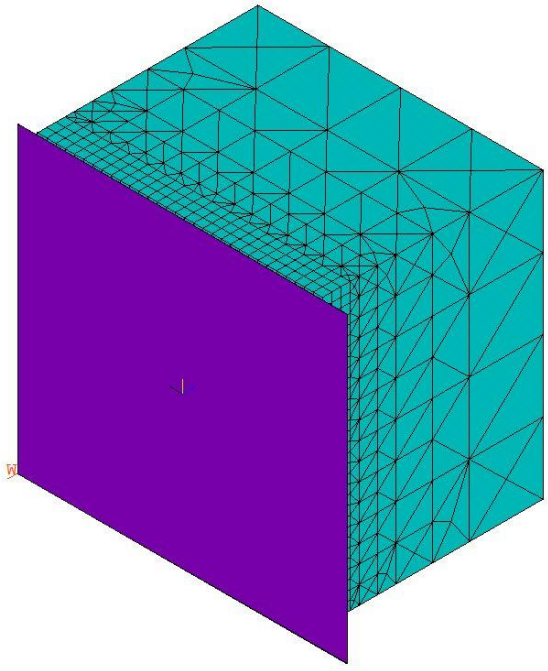

Figure 3.13 Meshed volume with target surface

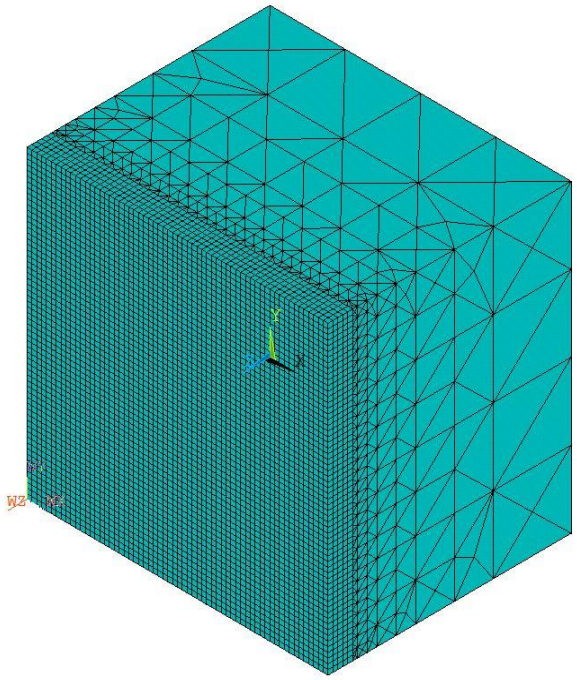

Figure 3.14 Meshed volume (63 by 63)

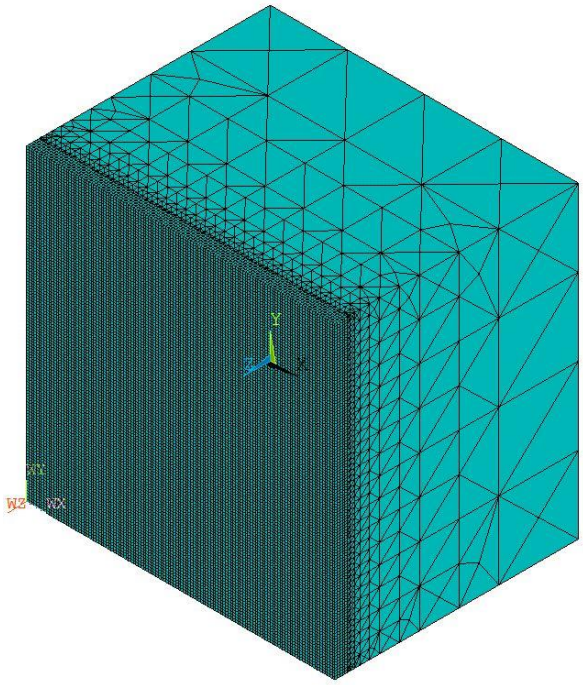

Figure 3.15 Meshed volume (125 by 125)

3.2.4.3 Moving Nodes To Create Roughness

A meshed rectangular volume (Fig. 3.16) is created after meshing. The coordinate in the Fig. 3.16 stipulates directions of *X*, *Y* and *Z*. Δx and Δy are the resolutions along the *X* and *Y* directions. Therefore, the next step is to add roughness to the surface.

Assuming that there is an arbitrary node, with the coordinates (*x*, *y*, *z*), located within the volume, the distance of moving of the node, d_z, is determined by the equation

$$d_z = Z(x, y)F(z) \tag{3.1}$$

where *Z(x, y)* is the rough surface height. *F(z)* represents a function of *z*. *F(z)* decreases progressively from one to zero as the value of *z* decreases from the dimension of thickness to the zero.

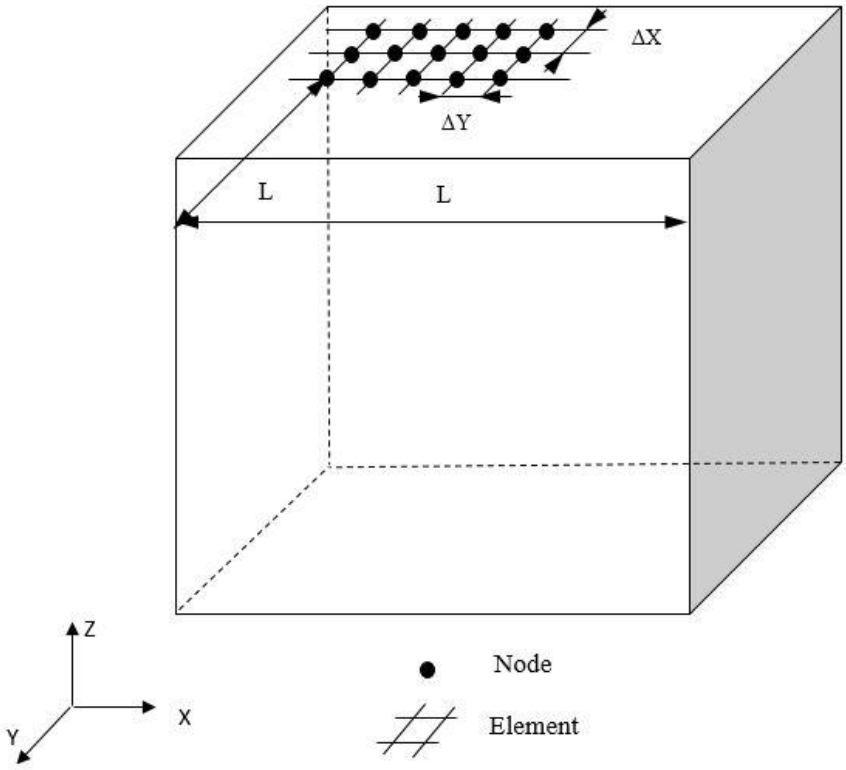

Figure3.16 Schematic expression of the meshed volume

The function *F(z)* varies with different models. Here is the equation used by Hyun et al [42]

$$d_z(x, y, z_0) = h(x, y)(L - z_0)^a \tag{3.2}$$

where z_0 is the initial height of all nodes. *h(x, y)* is the desired surface height. *a* is a constant which is set by users. Another alternative to Eq. 3.1 is given by

$$d_z = h(x, y)\left(\frac{z}{H}\right)^a \tag{3.3}$$

This is the equation used in Xu's [54] paper. *h(x, y)* is the rough surface height. *a* is a constant that is set by the users and H is the dimension between the top surface and the bottom surface. The amount of movement drops very quickly to zero from the top surface to the bottom surface.

In order to find a proper function of *F(z)*, the principle of badly distorted elements needs to be understood. Badly distorted elements can cause computational error in a finite element simulation and therefore impede convergence.

Ideally $\Delta x \approx \Delta y$ to reduce the distortion of an element. If the amount of movement is large relative to the resolution Δx and Δy, then the element may be badly distorted. The reasons that cause excessive element distortion are diverse, such as mesh qualities, poor aspect ratios of solid elements, material properties, or contact behavior. In order to prevent excessive element distortion, all of these reasons needed to be checked carefully. Generally, the maximum absolute value of the measured rough surface applied at each layer should be smaller than the resolution along the *X* direction (Δx) and *Y* direction (Δy).

Moving all the nodes within this cube would be unwise because the process would cost a very long period of time and resources. However, only moving nodes of the top layer would result in excessive element distortion, which may cause disconvergence of the model. Therefore, the nodes of only several layers were moved. The number of moved layers mainly depends on the resolution and the maximum absolute value of the rough surface. Three layers were used in the case of the 32 by 32 node surface (Fig. 3.12) and five layers were used in the 63 by 63 case (Fig. 3.14) and 125 by 125 case (Fig. 3.15). Therefore,

$$d_z = Z(x, y)\frac{n_i}{n_t} \tag{3.4}$$

where n_i represents the i_{th} layer and n_t represents the total number of layers in the model. The amount of movement of each layer is decided by the maximum absolute value of the original rough surface equally divided by the number of layers. Figs. 3.17, 3.18 and 3.19 represent the original 32 by 32 rough surface, the 63 by 63 rough surface and the 125 by 125 rough surface, respectively, in the simulation. After spectral interpolation, surfaces with more nodes also appear to become smoother.

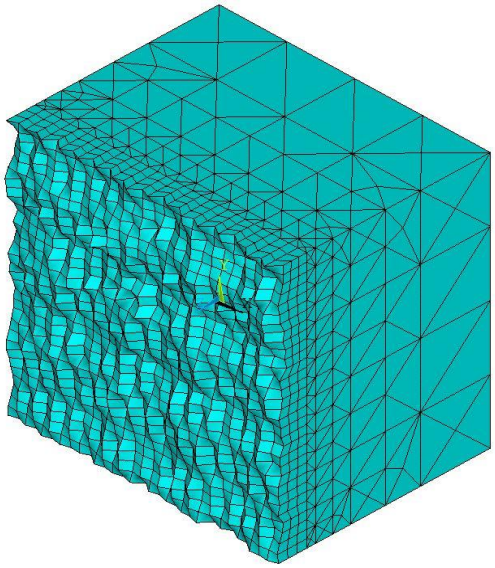

Figure 3.17 32 by 32 rough surface in ANSYS

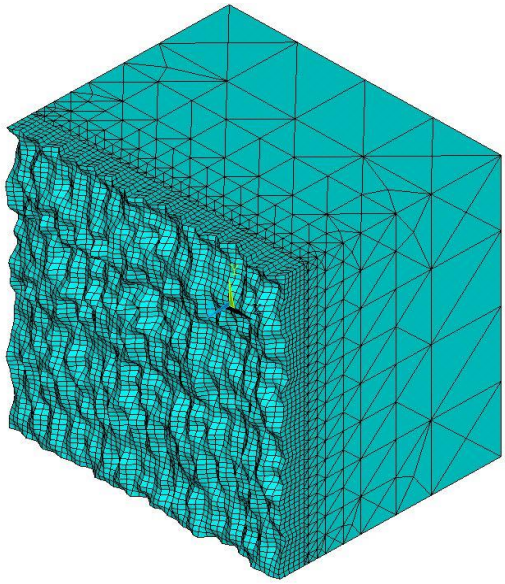

Figure 3.18 63 by 63 rough surface in ANSYS

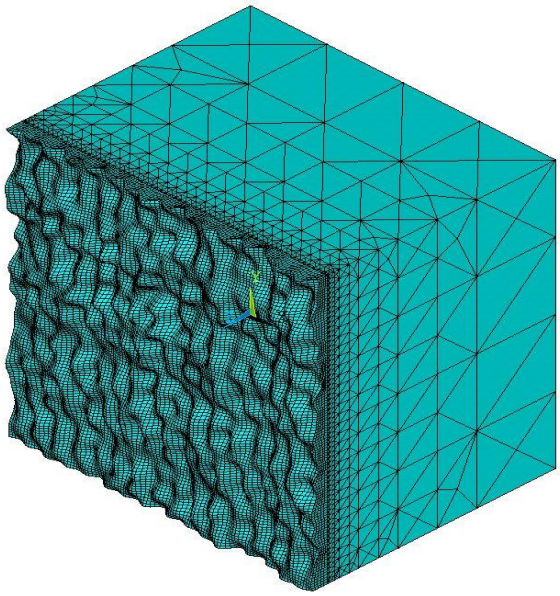

Figure 3.19 125 by 125 rough surface in ANSYS

3.2.5 Boundary Conditions

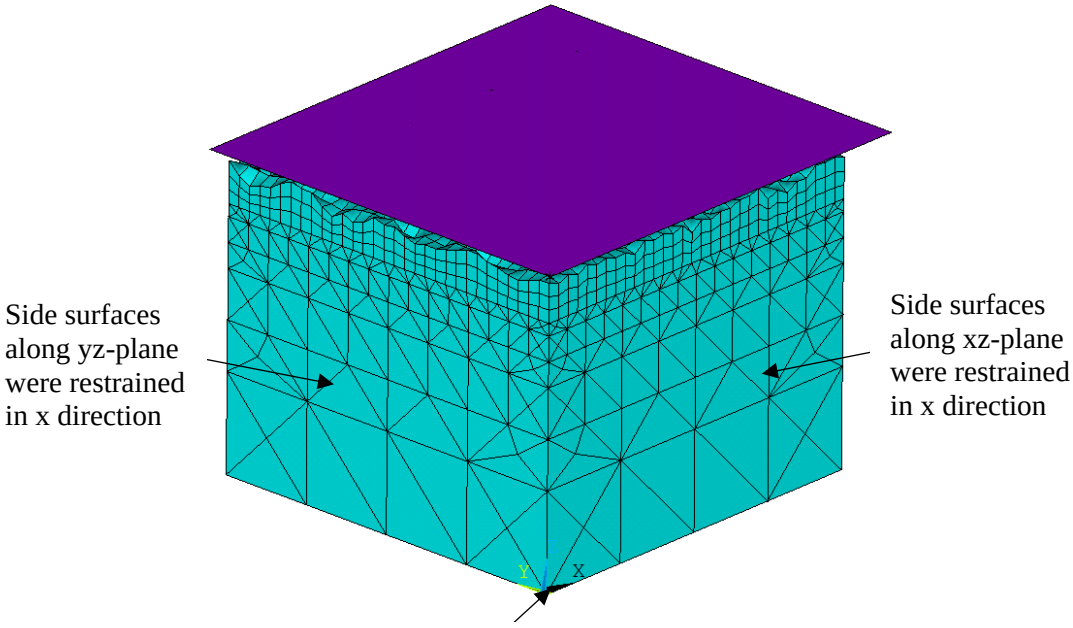

Figure 3.20 Boundary conditions

As shown in Fig. 3.19, all directions of displacement of the nodes associated with the bottom surface were set to zero. The displacement in the perpendicular direction on both side surfaces was constrained in order to enforce symmetry boundary conditions. Side surface areas along the *yz*-plane were restrained in the *x*-direction and the *xz*-planes were restrained in the *y*-direction.

3.3 Summery

In this chapter, details of the numerical simulation are discussed. First, the data of the measured rough surface is processed by the spectral interpolation. Therefore, the original 32 by 32 node surface is enlarged to a 63 by 63 node surface at the first interpolation, and to a 125 by 125 node surface at the second interpolation. Then, these rough surfaces are used to create contact models in the commercial software $ANSYS^{TM}$ by using the finite element method. Detailed information about these models are introduced, such as element selection, material properties and mesh generation. Next, the symmetry boundary conditions are applied in the simulations. Through the simulations of the contact model, many problems can be studied, such as the effects of the tangential modulus, the influence of different locations of the detection point and the real contact area. Studies of these problems will be presented in Chapter 4.

Chapter 4

Results and Comparison

In this chapter, we studied the resolution effects on the relationship between the real contact area and the contact load. The FEM results are then compared to several theoretical models. We also analyzed the hardening effects on the area-load relationship and options of the contact detection point.

4.1 Hardening Effects

Strain hardening is an important plastic deformation behavior that has been researched very little. In 2006, Brizmer et al. [56] found that the change of the tangential modulus, from 2% to 0.2% for instance, only slightly affects the results in the elastic-plastic spherical contact problems. Their studies in 2007 [57] and Zolotarevskiy et al. [58] in 2011 also made the same suggestions about the value of the tangential modulus. However, this conclusion of Brizmer et al. might not be correct in the condition of rough surface contact. In order to characterize the effects of the tangential modulus on the rough surface contact problems, we ran a series of simulations with the same rough surface and same parameters except for the value of tangential modulus.

The area with 32 by 32 nodes that was introduced in the Chapter 3 was used for the analysis. This area is extracted from the surface 4L. Seven cases were run in total based on the area. All the parameters are the same, such as the elastic modulus (200GPa) and the Poisson's ratio (0.3) except the value of the tangential modulus. The value was changed from 0MPa (0%) to 4GPa (2%)

progressively in order to find the effects of the tangential modulus on the area-load relationship. The 0% case is the elastic-perfectly plastic case.

Table 4.1 presents the related parameters of the rough surface and Fig. 4.1 shows the comparison of the area-load relationship between the seven cases. As the value of the tangential modulus decreases from 4000MPa to 0MPa, the trends of these lines are approaching to the 0% line gradually. The 2% line is the most gradually increasing line and the 0% line is the steepest line.

	1	2	3	4	5	6	7
Tangential modulus, Et	0MPa	100MPa	200MPa	500MPa	1000MPa	2000MPa	4000MPa
Percentage of elastic modulus	0%	0.05%	0.1%	0.25%	0.5%	1%	2%

Table 4.1 Tangential modulus value of seven cases

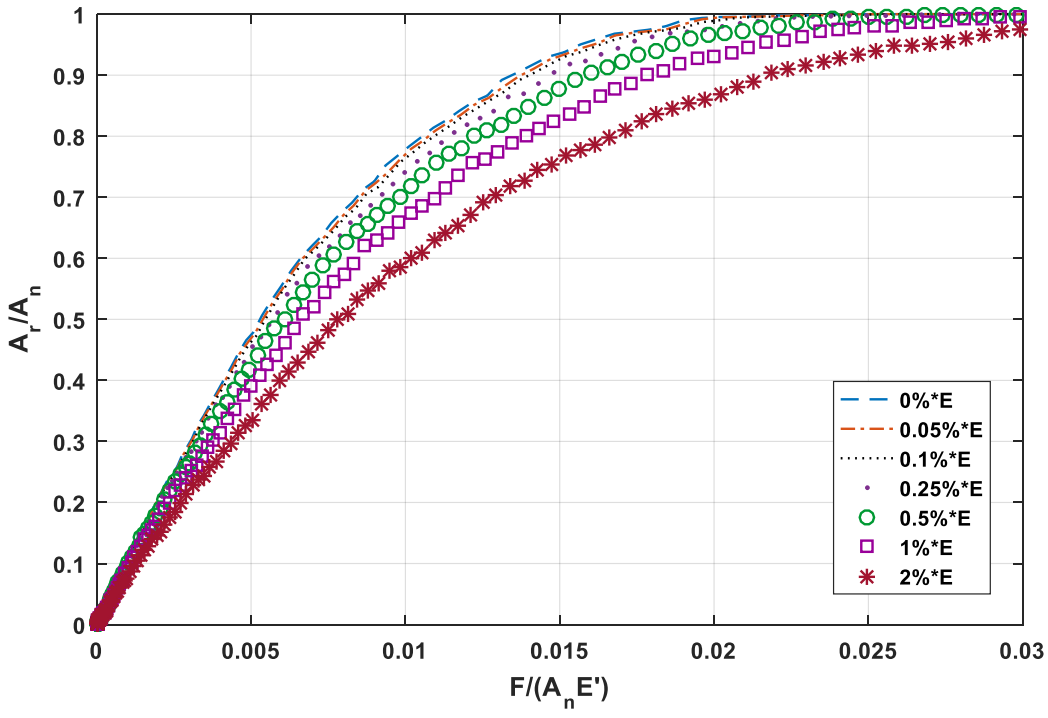

Figure 4.1 Harding Effects

According to Fig. 4.1, there is an obvious difference between the 2% line and the 0% line. If the value of tangential modulus of a material is equal to zero, then it is called the elastic-perfectly plastic material. After the value of stress reaches the yield strength, stress does not increase with further deformation, thus the elastic-perfectly plastic material is the more idealistic and fundamental case. However, zero tangential modulus will largely increase the convergence difficulty. Therefore, we choose $Et = 100MPa$, which is 0.05% percent of the value of elastic modulus, as the value of tangential modulus for all simulations in the current thesis. The average error of the 100Mpa case only differs by 0.14% from the elastic-perfectly plastic case.

4.2 Contact Detection Point

In general, Gauss integration points are used as contact detection points for surface-to-surface contact elements. Since the finite element model in the current thesis is used to simulate interactions between a rough surface and a rigid flat surface, we used the ANSYS default setting initially (Gauss integration points). However, we found that the contact between rough surfaces is not portrayed well by the condition of surface to surface contact.

In fact, from a micro-scale point of view, the asperity peaks are first in contact with the rigid flat surface, which create many corner contacts at the initiation of contact. If asperities are very smooth, the value of initial penetration is very small, thus can be neglected. However, If asperities are steep, then the value of initial penetration will be very large, which may affect the correctness of the results. (Fig. 4.2) Therefore, the nodal points was used to replace the original Gauss integration points as the location of contact detection points.

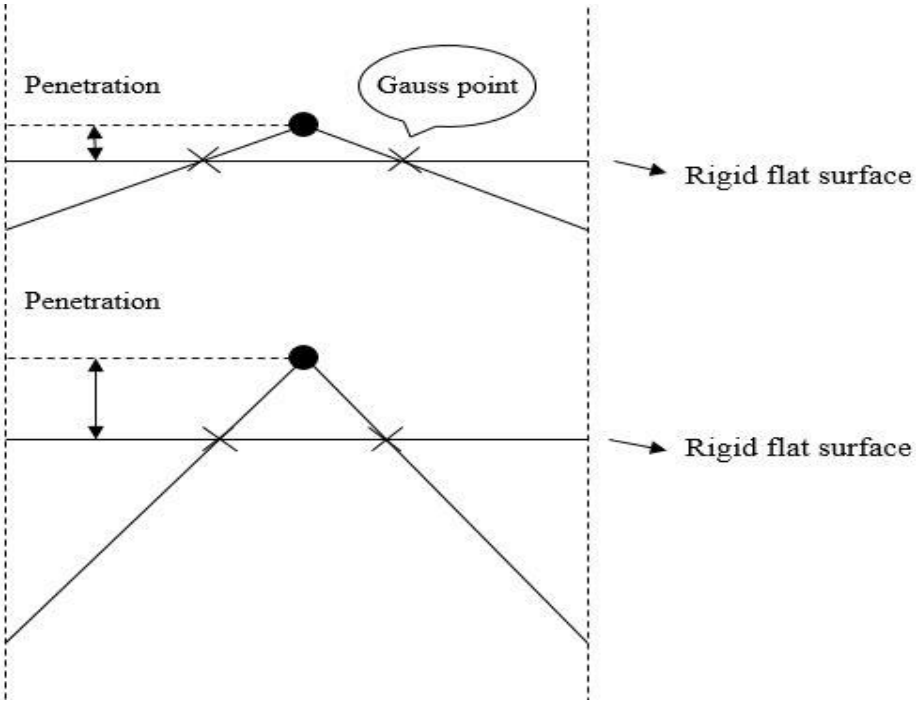

Figure 4.2 Gauss integration points

In order to validate the correctness of the nodal detection algorithm, we compared six perfectly elastic cases including both conditions of contact detection to the results obtained from the boundary element method [53]. Table 4.2 introduces the options of detection points of the six cases. The value of elastic modulus and Poisson's ratio of all cases are 200GPa and 0.3, respectively. Fig. 4.3 shows the comparison of the area-load relationships between the boundary element method and the two contact detection conditions. The nodal point case of 125 by 125 nodes is the closest line to the BEM results.

Number of nodes	32 × 32	63 × 63	125 × 125	32 × 32	63 × 63	125 × 125
Options of detection points	Nodal points	Nodal points	Nodal points	Gauss points	Gauss points	Gauss points

Table 4.2 Options of detection points of the six elastic cases

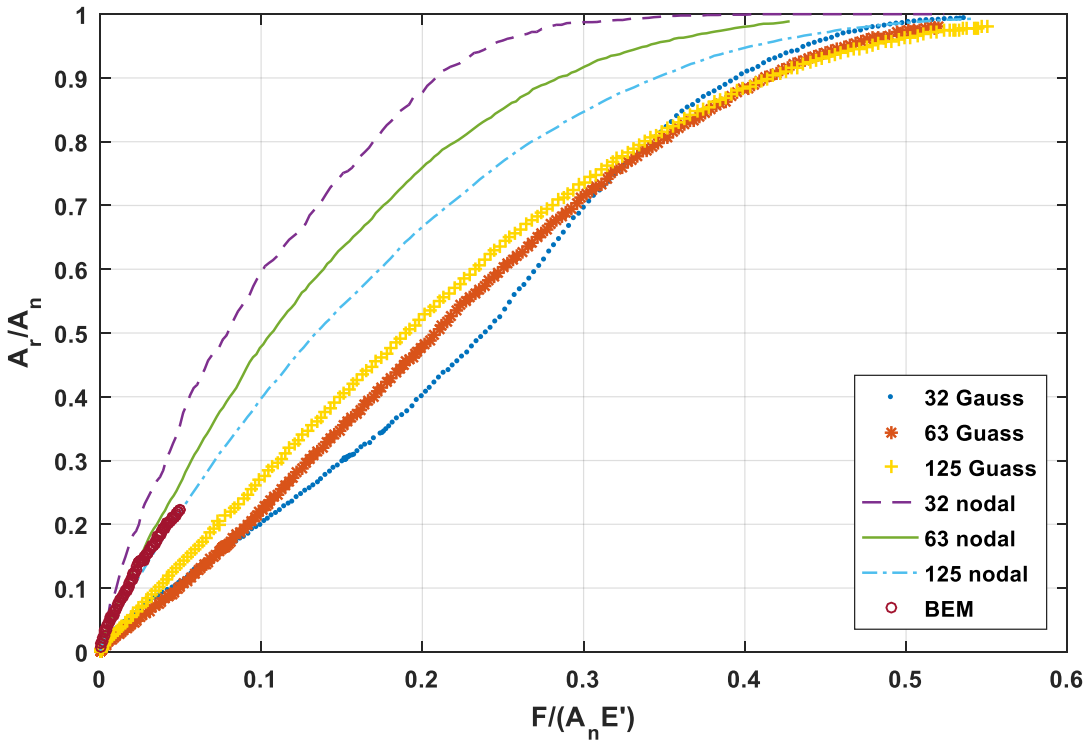

Figure 4.3 Comparison with BEM results

4.3 Resolution Effects

The method of spectral interpolation is described in full detailed in Chapter 3. The number of nodes within the extracted square area was increased from 32 by 32 to 63 by 63 at the first interpolation and to 125 by 125 at the second interpolation by using this method. Meanwhile, the nominal contact area and the surface spectrum remains constant. These processes leads to the interval between two consecutive nodes decreased from one micrometer to 0.5 micrometer and 0.25 micrometer.

With the surface data of these three conditions, we are able to build elastic-plastic finite element models to simulate interactions between rough surfaces and a rigid flat surface. Material properties of both cases include the elastic modulus (200GPa), Poisson's ratio (0.3) and yield stress (1Gpa).

The effects of different resolutions on the relationship between the real contact area and the contact load can be seen in Fig. 4.4. There is an obvious difference between the original surface and the spectrally interpolated surfaces. With increasing interpolation, the slope of the area-load relationship becomes lower, and the real contact area decreases overall.

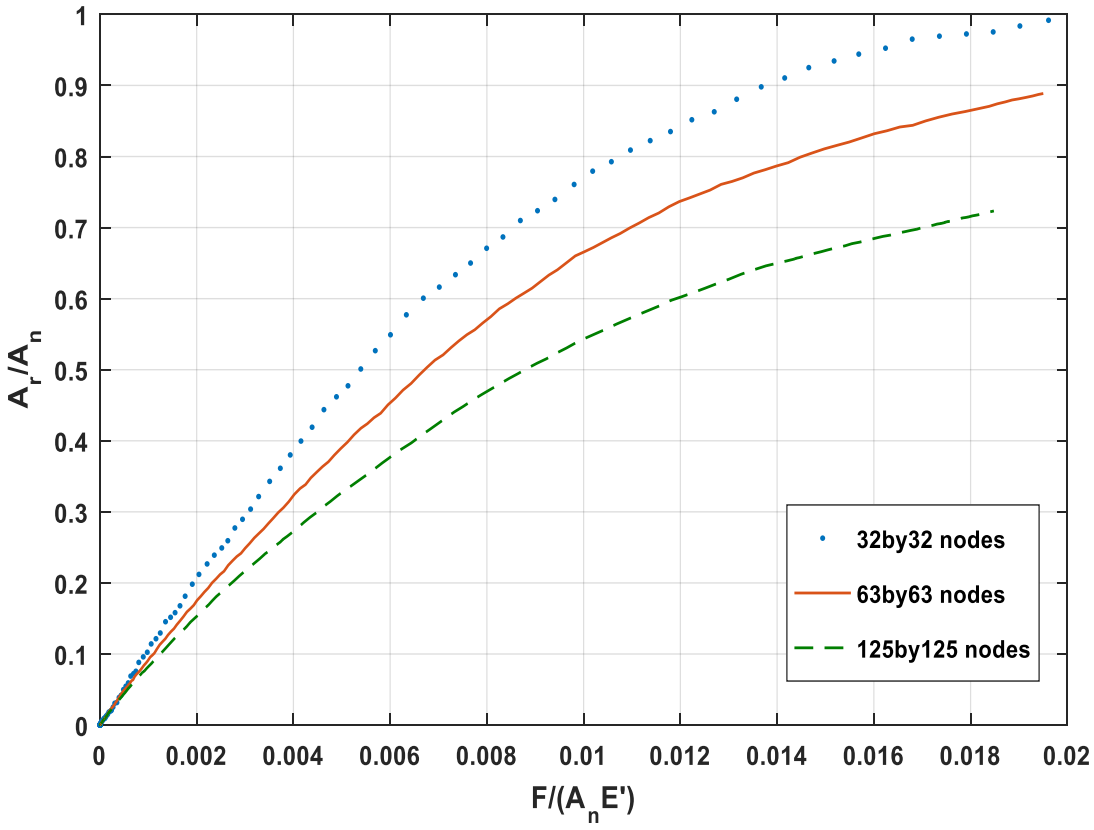

Figure 4.4 Comparison between the original surface and two interpolated surfaces

4.4 Comparison to Theoretical Models

Fig. 4.5 represents the comparison between the interpolated case with 125 by 125 nodes and theoretical models, such as the hardness model [4], Hyun and Robbins' model (HR) [43], MB model [28], Jackson's simplified multiscale model [38] and Wilson et al.'s full multiscale model [34]. The equations and the parameters of theoretical models are introduced at chapter two. The

hardness $H = s_y$, the value of B_{max} is 0.0408, the fractal dimension D and the fractal roughness parameter G are 1.917 and 5.439e-10 m, respectively.

The trends of theoretical models are basically in agreement with the finite element results, but there are large quantitative differences. The predictions of the FEM results is between the predictions of full multiscale model and the simplified multiscale model. The predictions of the hardness model, the Hyun and Robbin's model and the MB model predictions are much larger than the FEM results. The reason of this phenomenon is because that the MB model used a truncation based fractal model which may not capture the contact meaning correctly. Furthermore, Hyun and Robbins' model is merely a fit to FEM results and is not based on fundamental mechanics.

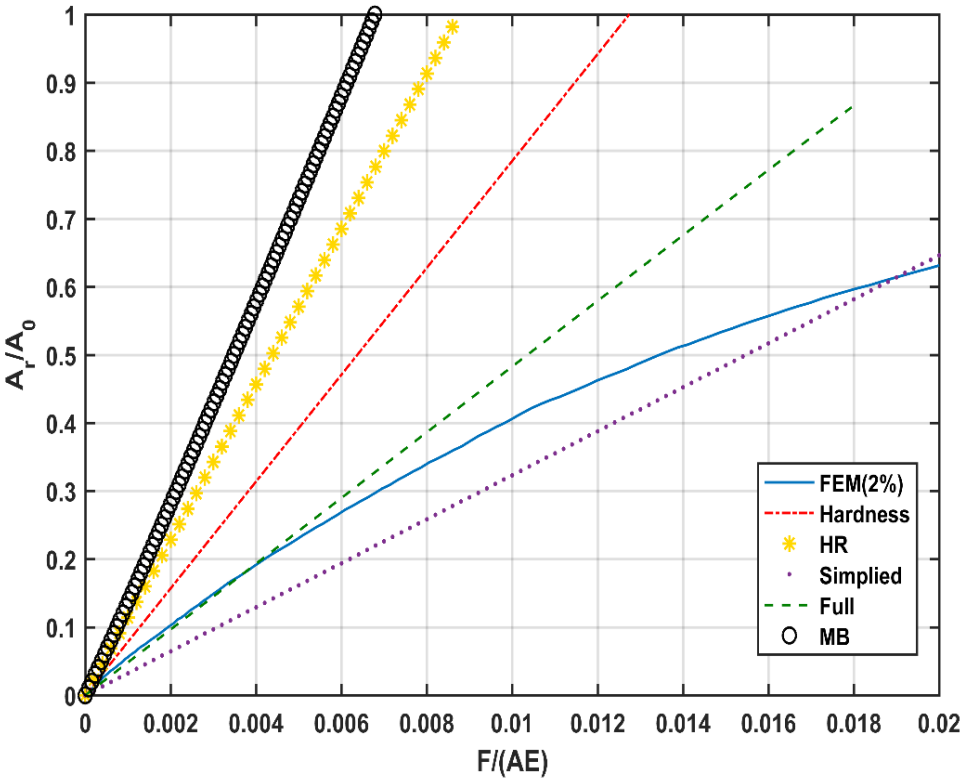

Figure 4.5 Comparison with theoretical models

In order to quantify the repeatability and sensitivity, the finite element model results are compared for different areas in the same surface and also for different surfaces. The measurement of rough surfaces are introduced in the Chapter 1. In total, three rough surfaces are measured by an optical profilometer, 4L, 8G and 16G. The measurement size of each original surface is 1023um by 1023um (1024 by 1024 nodes). The first area considered in this work was extracted from the surface 4L.

First, five different square areas with the same size as the original area are randomly chosen from the same measured surface (4L). These five areas are processed the exact same way as the original extracted square area was processed by the method of spectral interpolation. Only the 125 by 125 node cases are compared. Fig. 4.6 describes the locations of the five areas in surface 4L. Table. 4.3 present the roughness parameters of these five areas and the original area. Fig. 4.7 present the surface spectrum of the five areas from surface 4L and the original area. With the increase of the wavelength, the value of amplitude increases slightly and the ratio between amplitude and wavelength decreases rapidly. Fig. 4.8 shows the comparison between the original area and the five areas in surface 4L. The general trend of the area-load relationship of these six areas is basically the same. However, the line of 4L4 deviates a little bit from the other lines. This phenomenon can be explained by Fig. 4.9, which describes the relationship between R_q and the contact area ratio. The R_q value of the area 4 in surface 4L is the largest of all other areas. In many cases, but not universally, contact area decreases with surface roughness. Therefore, the area-load relationship of area 4 is lower than other areas because it has a much larger roughness. The results of one area, 4L5, is selected to compare with the theoretical models described in Fig. 4.10. The condition of the comparison is very similar to the previous one except slightly difference of slopes.

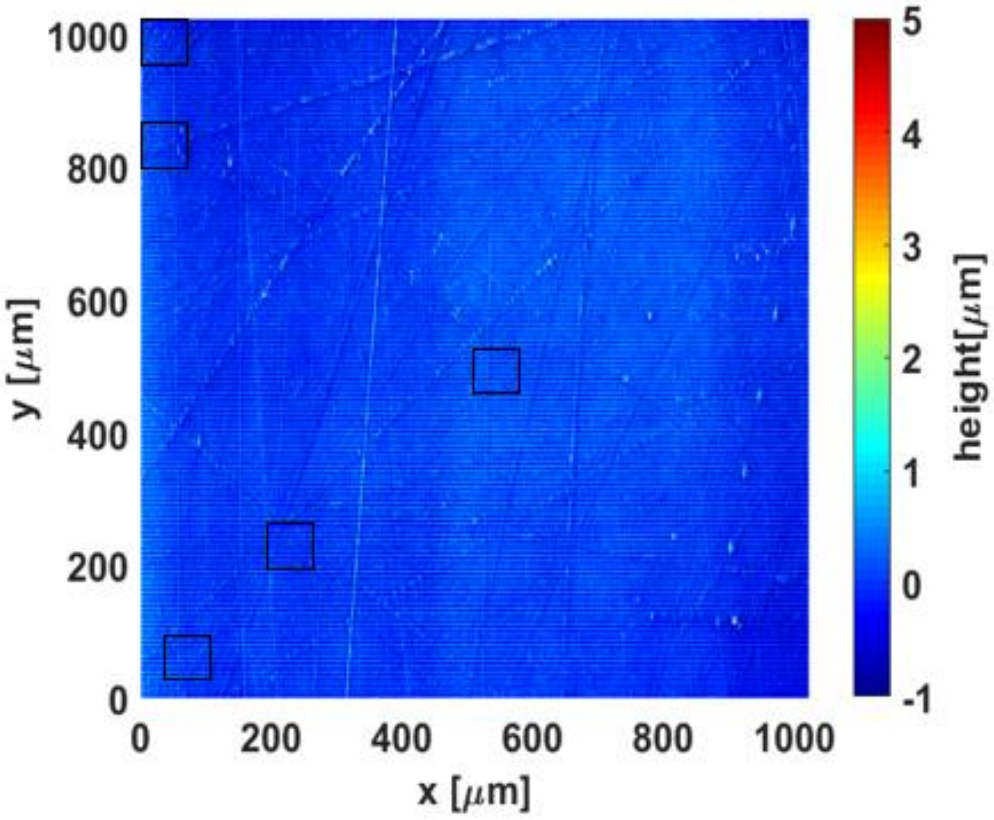

Figure 4.6 Locations of the five areas in measured surface 4L

	Original	Area 1	Area 2	Area 3	Area 4	Area 5
Ra	3.5586e-7	2.4488e-7	2.6044e-7	3.0342e-7	4.2524e-7	3.5136e-7
Rq	4.3179e-7	2.9446e-7	3.1765e-7	3.1765e-7	4.9109e-7	4.2902e-7

Table 4.3 Surface roughness of the five areas in 4L and the original area

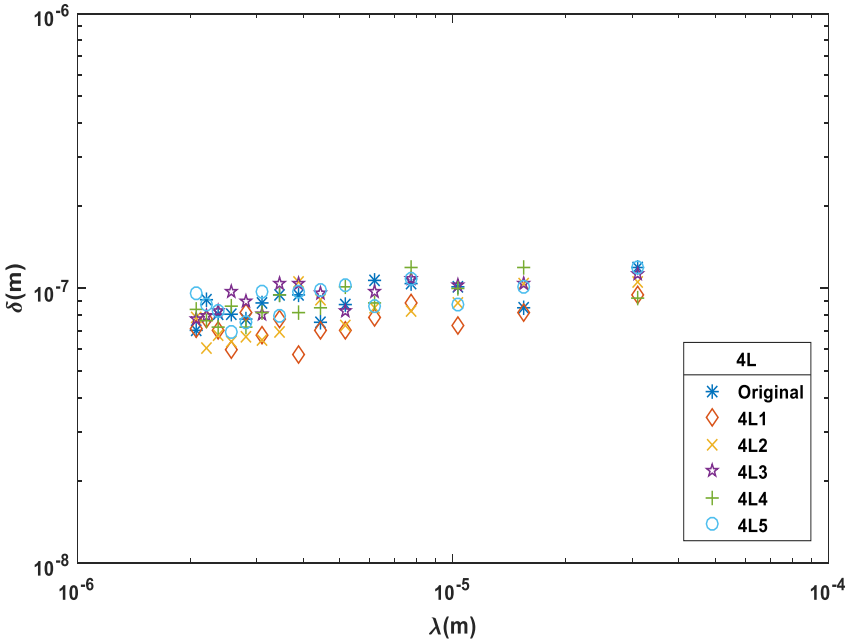

(a)

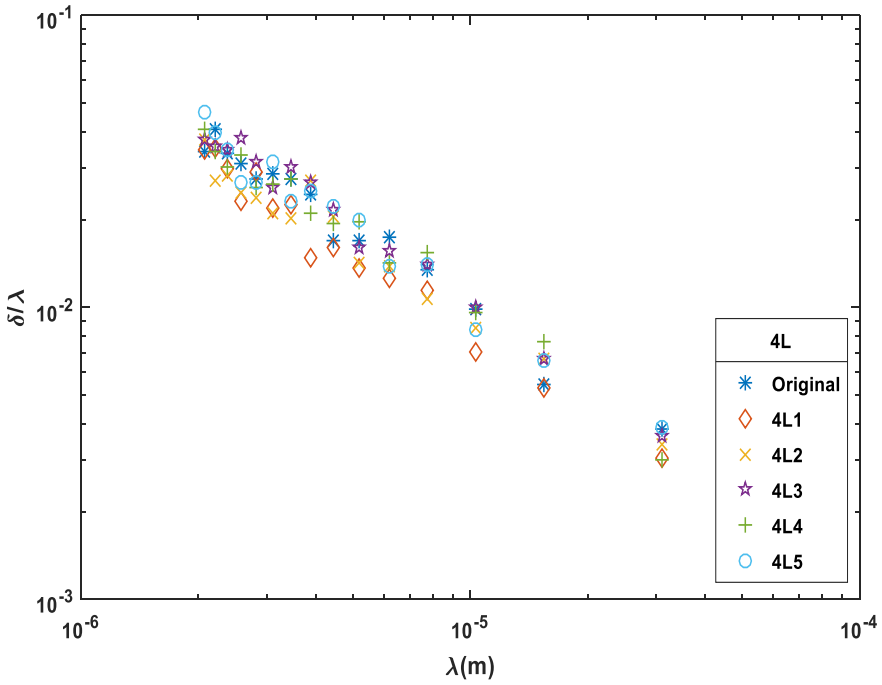

(b)

Figure 4.7 (a) Resulting amplitude versus wavelength curve for surface 4L | (b) Resulting amplitude/wavelength versus wavelength curve for surface 4L

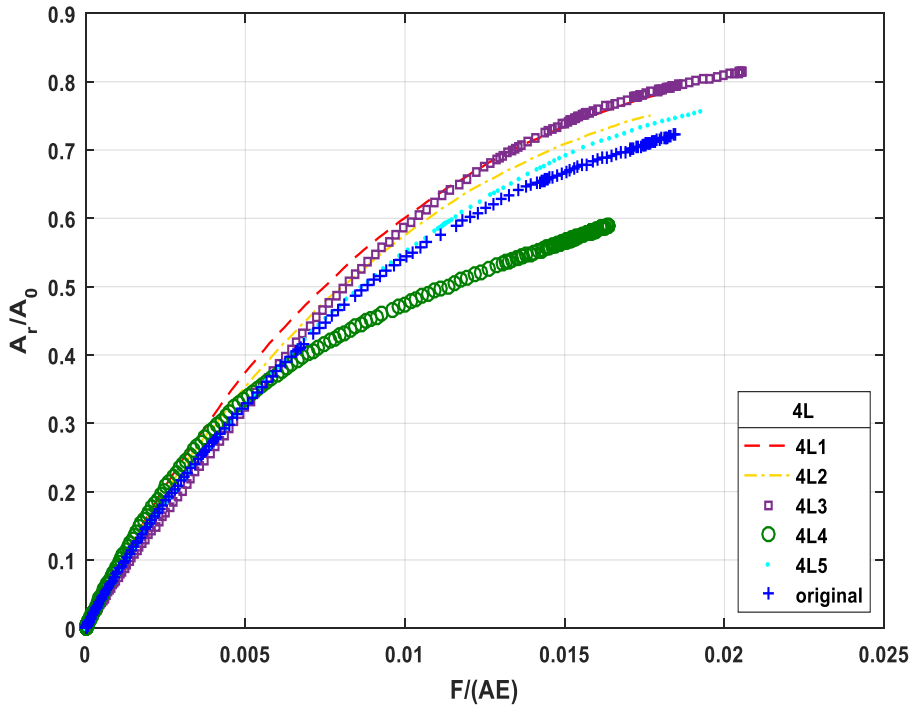

Figure 4.8 Comparison between the original area and the five areas from surface 4L

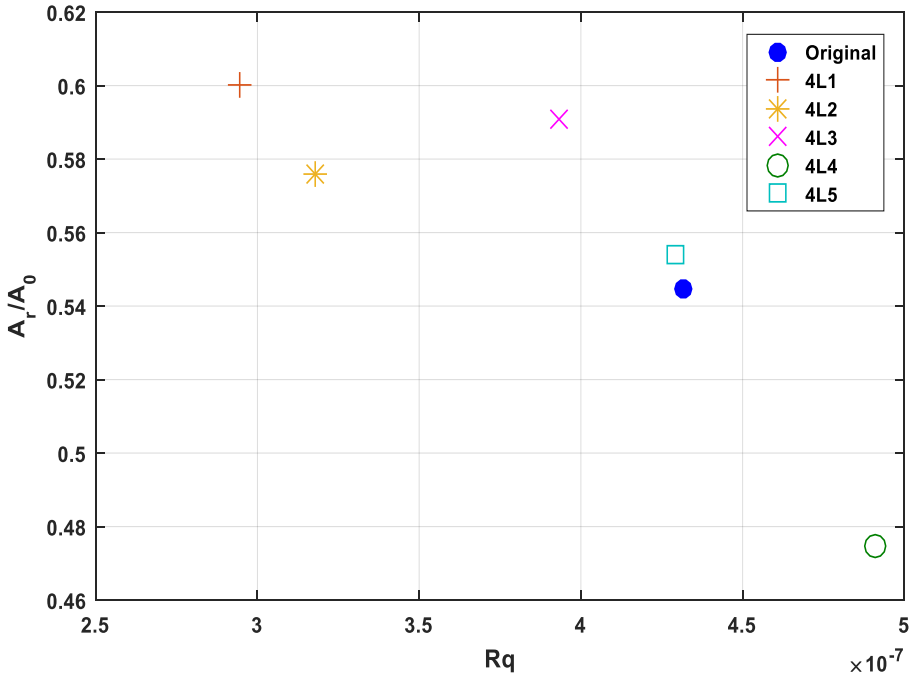

Figure 4.9 Relationship between R_q and contact area ratio of the five areas in surface 4L

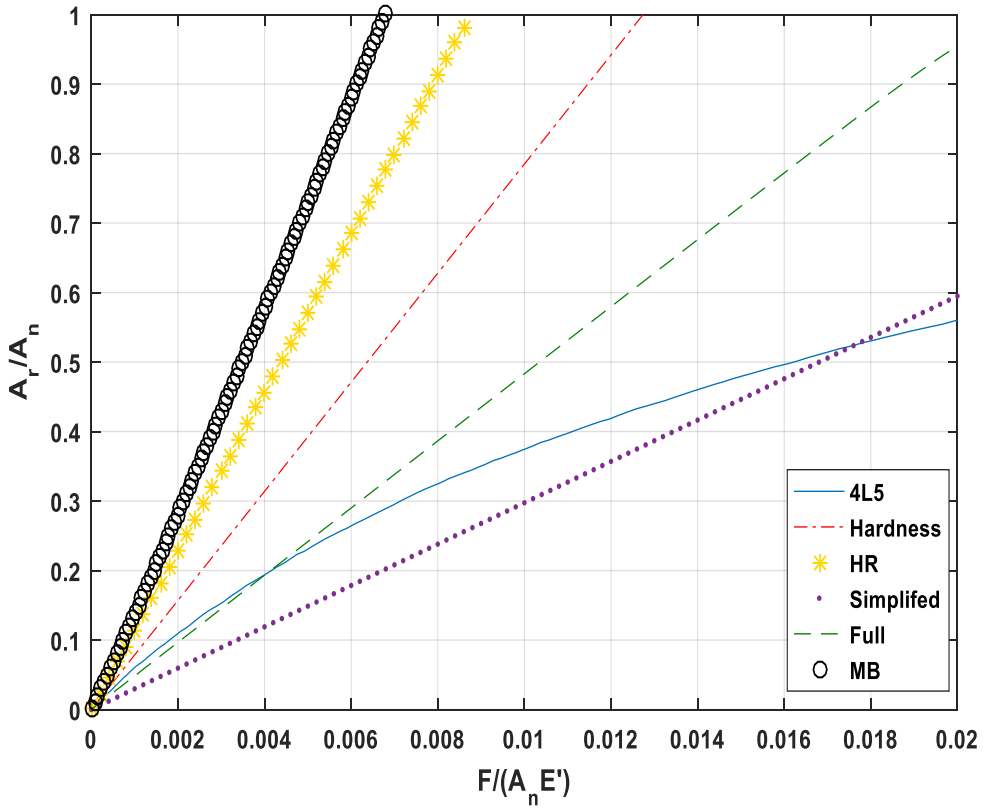

Figure 4.10 Comparison with theoretical models (4L5)

Second, three different square areas with the same size as the original area are randomly chosen from the measured surface 8g and 16g, respectively. Both of these areas are also processed by the exact same method. Only the spectrally interpolated 125 by 125 node cases are compared. Fig. 4.11 and 4.12 describes the locations of these six areas in the measured surface 8g and 16g. Table. 4.4 presents their roughness parameters. Fig. 4.13 and 4.14 present the surface spectrum of the six areas compared with the original area. With the increase of the wavelength, the value of amplitude increases slightly and the ratio between amplitude and wavelength decreases rapidly. Fig. 4.15 and 4.16 show the comparison between the original area and the three areas that come from the measured surface 8g and 16g, respectively. In Fig 4.15, the line of the original area and the lines of the 8g2 and 8g3 agree well whereas the line of the 8g1 is deviated a little. In Fig 4.16, the line

of 16g2 and the original area converges while the lines of 16g1 and 16g3 converges. Fig. 4.17 and 4.18 can explain these convergence conditions. The principles are very similar to the previous explanation of area 4 in surface 4L. The R_q value of the 8g1 is smaller than the others, so the contact area is larger. The R_q value of the original area and 16g2 are close to each other while the R_q value of the 16g1 and 16g3 are also close to each other. Therefore, the corresponding slopes of the original area and 16g2 agree well, while the 16g1 and 16g3 agree well. The results of one area from each surface, 8g3 and 16g3, are selected to compare with the theoretical models described in Fig. 4.19 and 4.20. The results of the comparisons are very similar to the previous one for surface XX, except for slightly different slopes and overall values of contact area. Again, the multiscale models appear to compare the best to the FEM results relative to the other model.

The resolution effects are mainly analyzed in this section. We found that with increasing interpolation, the slope of the area-load relationship becomes lower. The FEM results are then compared to theoretical models. We also found two interesting places in the process of researching. First, the value of tangential modulus will affects the area-load relationship even under 2% of the elastic modulus. Second, nodal points are more reasonable then Gauss points to be used as contact detection points.

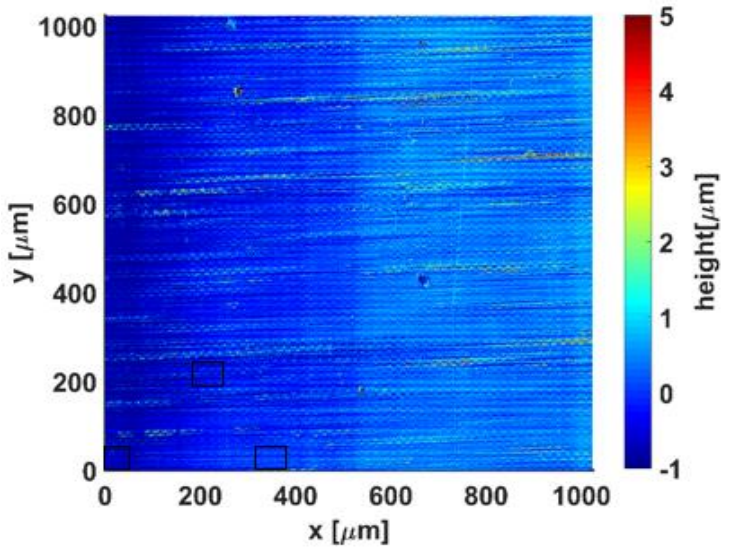

Figure 4.11 Locations of the six areas in measured surface 8g

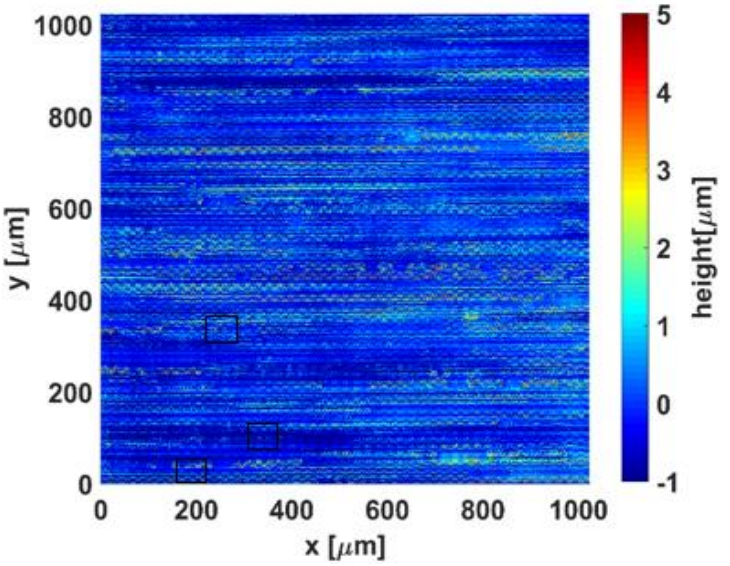

Figure 4.12 Locations of the six areas in measured surface 16g

	8g1	8g2	8g3	16g1	16g2	16g3
Ra	1.8702e-7	3.3598e-7	2.8282e-7	5.8510e-7	3.3814e-7	6.1072e-7
Rq	2.4320e-7	4.2497e-7	3.6621e-7	7.4786e-7	4.4457e-7	7.6767e-7

Table 4.4 Surface roughness of the six areas in 8G and 16G

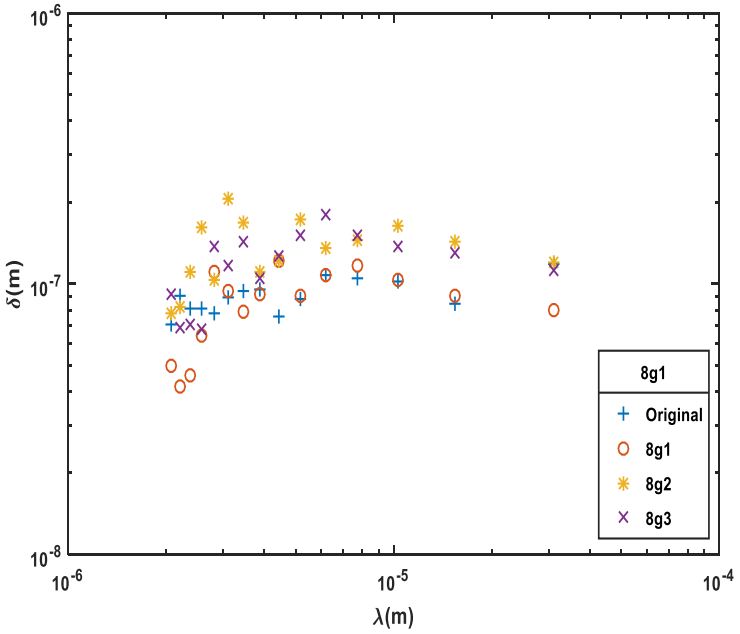

(a)

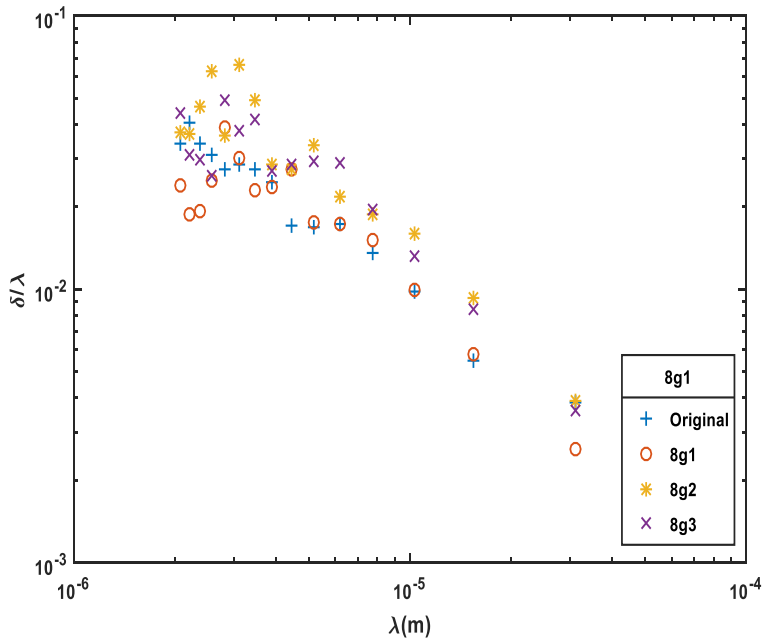

(b)

Figure 4.13 (a) Resulting amplitude versus wavelength curve for surface 8G | (b) Resulting amplitude/wavelength versus wavelength curve for surface 8G

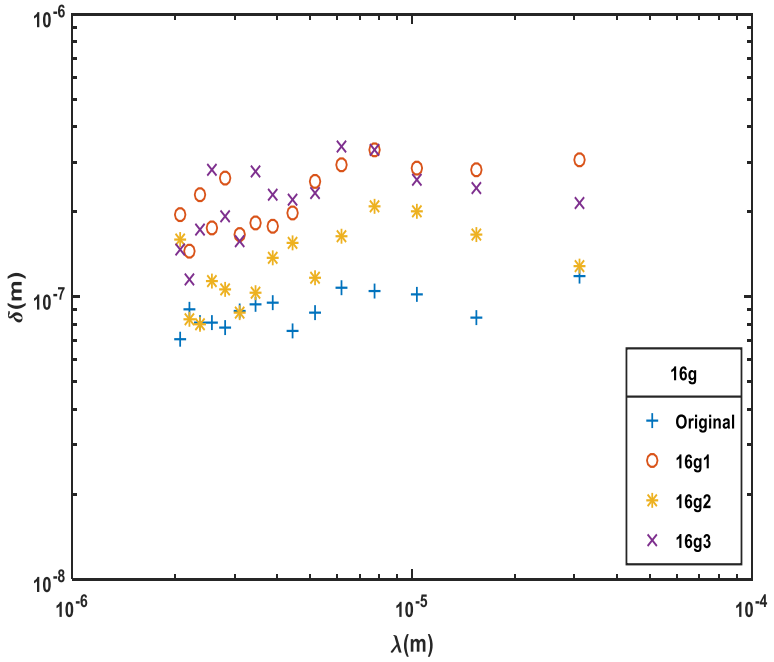

(a)

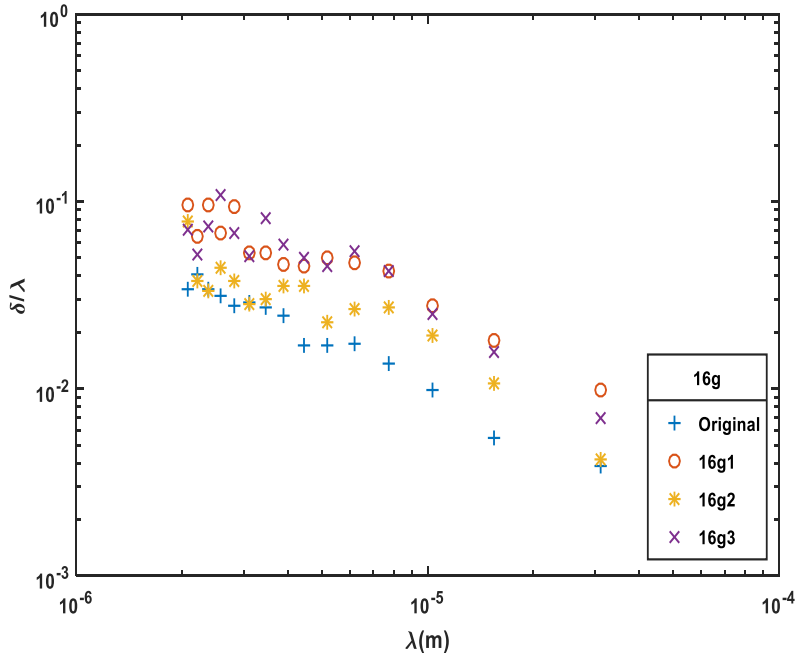

(b)

Figure 4.14 (a) Resulting amplitude versus wavelength curve for surface 16G | (b) Resulting amplitude/wavelength versus wavelength curve for surface 16G

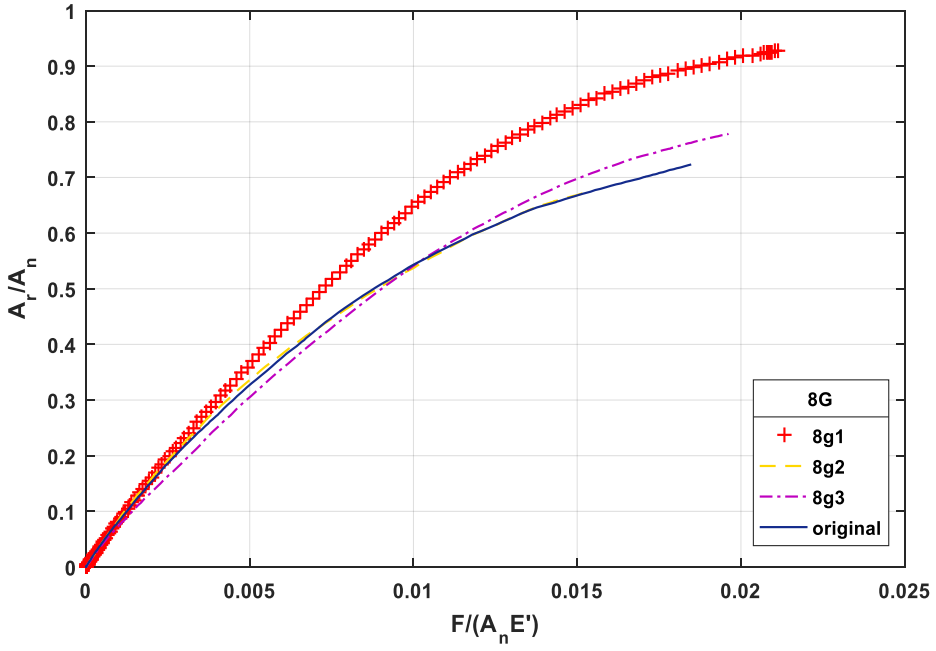

Figure 4.15 Comparison between the original area and the three areas from 8G

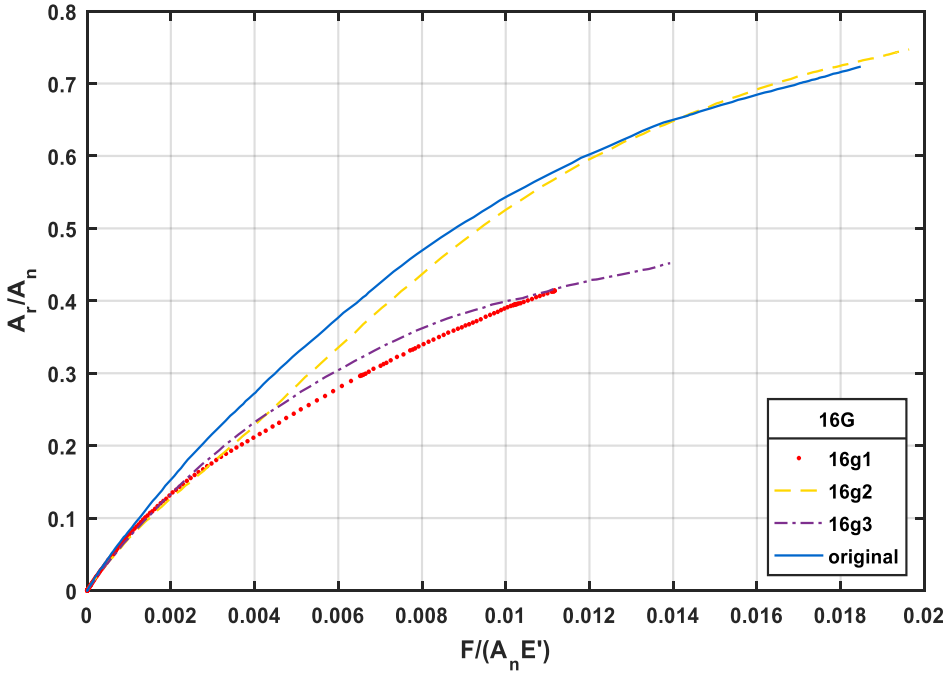

Figure 4.16 Comparison between the original area and the three areas from 16G

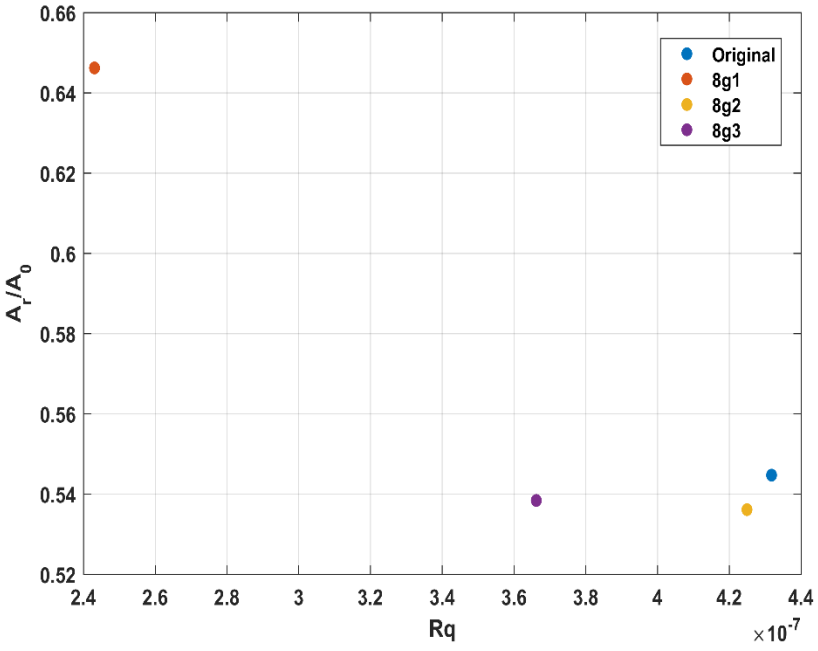

Figure 4.17 Relationship between R_q and contact area ratio of the three areas in surface 8g

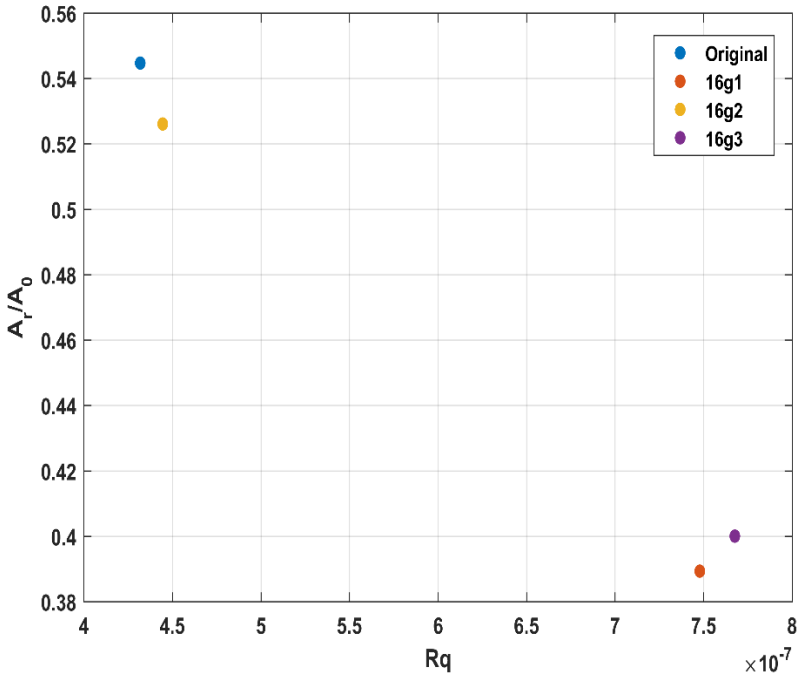

Figure 4.18 Relationship between R_q and contact area ratio of the three areas in surface 16g

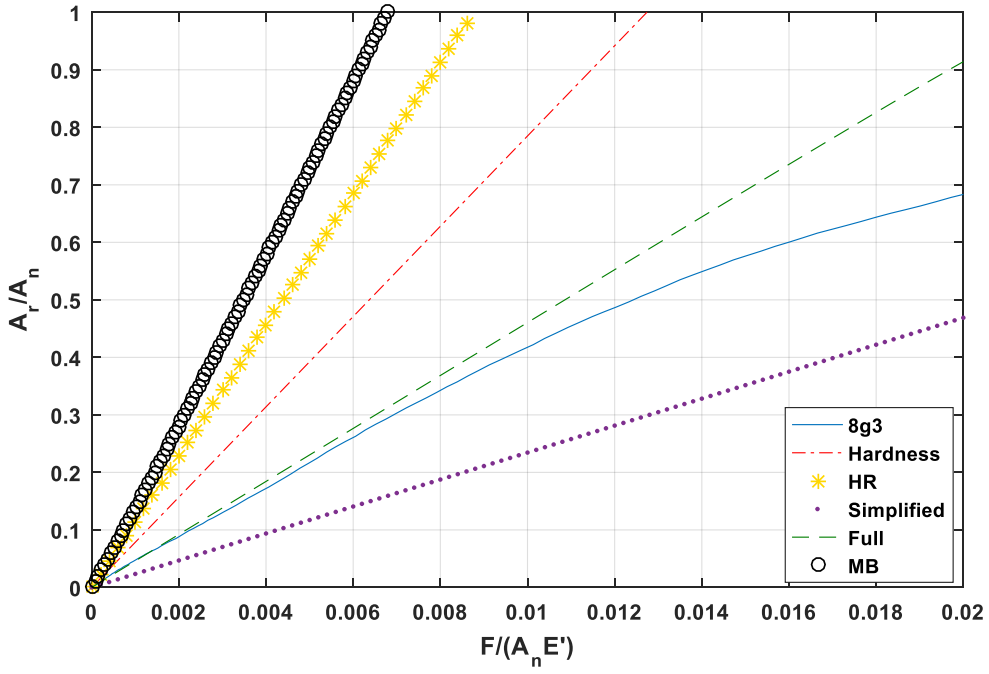

Figure 4.19 Comparison with theoretical models (8g3)

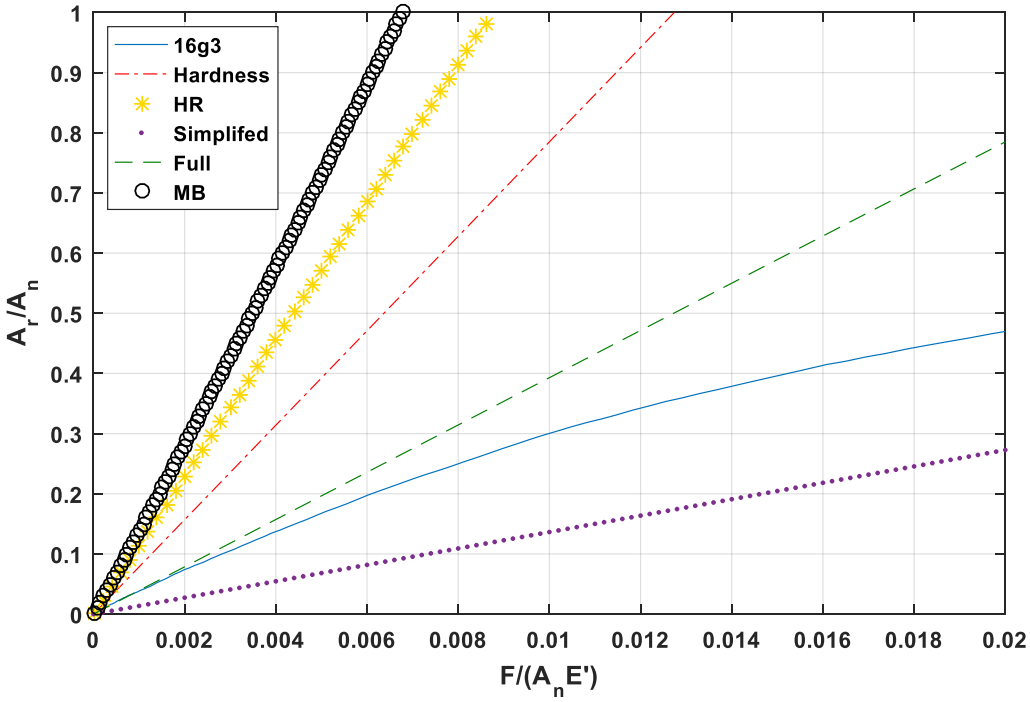

Figure 4.20 Comparison with theoretical models (16g3)

Chapter 5

Conclusions

Rough surfaces are very common in the real world. From a microscopic point of view, interactions between these rough surfaces are actually happening between peaks or asperities. Asperities of real surfaces are usually not sharp peaks but more rounded or curved. However, previous studies of rough surfaces are frequently ignoring this point. Linear relationships are always assumed between two consecutive nodes, which leads to jagged triangular or pyramidal geometries. The spectral interpolation method that is used in the current thesis allows for sharp peaks and intermediate points to be smoothed by adding additional nodes. Therefore, the linear relationship between two consecutive nodes is replaced by a harmonic relationship. Meanwhile, the surface spectrum and the nominal contact area remains constant.

The results of the FEM simulation in Fig. 4.5 shows that the slope of the area-load relationship becomes lower as the geometry of the rough surface was smoothed by the spectral interpolation. Each area is interpolated two times in total. The area-load relationship will continue to change with interpolations at higher frequencies until they converge to a solution. However, due to the limited computational ability, third divisions of interpolation takes incredibly large times to execute. This problem will be alleviated in the future. The results were compared to theoretical models, such as the hardness model, HR model, MB model and multiscale model. They are in qualitative agreement but disagree quantitatively. The multiscale model shows the best agreement.

We also extracted five other areas from the surface 4L and three areas each from the surfaces 8G and 16G. These areas possess exactly the same resolutions and same total nodes. They also are smoothed by the spectral interpolation method. Their results are compared to the results of the original area from the surface 4L. The majority of the results agree well whereas a few of them are deviated a little bit because of the difference of roughness.

In the process of refining the results shown in this work, we found two places that the can be improved. The first place is the tangential modulus. Its value was set at 2 percent of the elastic modulus initially. However, we found that this value puts an obvious hardening effect on the simulation results compared with the value of 0% percent, which is the value of an elastic-perfectly plastic material. The elastic-perfectly plastic material is not realistic, therefore, we treat the material as a fundamental case in our theoretical researches. Since the programs will be hard to converge with the 0% percent value, we adopt 100Mpa, which is 0.05% percent of the elastic modulus, as the value of the tangential modulus.

The other place of improvement is the contact detection point. It is the fourth key option of the contact element CONTA 173 in ANSYS. Firstly, Gauss integration points were used because it is an appropriate option for surface to surface contact. However, this option allows very large initial penetrations. Many corner contacts are created at the top of asperities during the early contact period. Therefore, nodal points are used as contact detection points instead of Gauss integration points. To verify its correctness, these two options are compared to boundary element results and Fig. 4.4 proves that the nodal point option is more effective.

Reference

[1]. Johnson, K. L. "Contact mechanics, 1985." (1974): 57-63.

[2]. Williams, John. Engineering tribology. Cambridge University Press, 2005.

[3]. McCool, J. I. "Relating profile instrument measurements to the functional performance of rough surfaces." Journal of Tribology 109.2 (1987): 264-270.

[4]. Bowden, Frank Philip, and David Tabor. The friction and lubrication of solids. Vol. 1. Oxford University Press, 2001.

[5]. Abbott, E. J., and F. A. Firestone. "Specifying surface quality: a method based on accurate measurement and comparison." SPIE MILESTONE SERIES MS 107 (1995): 63-63.

[6]. Greenwood, J. A., and JB Pl Williamson. "Contact of nominally flat surfaces." Proceedings of the Royal Society of London A: Mathematical, Physical and Engineering Sciences. Vol. 295. No. 1442. The Royal Society, 1966.

[7]. Greenwood, Jim A., and J. Hl Tripp. "The elastic contact of rough spheres." Journal of Applied Mechanics 34.1 (1967): 153-159.

[8]. Greenwood, J. A., and J. H. Tripp. "The contact of two nominally flat rough surfaces." Proceedings of the institution of mechanical engineers 185.1 (1970): 625-633.

[9]. Hisakado, T. "Effect of surface roughness on contact between solid surfaces." Wear 28.2 (1974): 217-234.

[10]. Onions, R. A. and J. F. Archard (1973). "Contact of Surfaces Having a Random Structure." Journal of Physics D-Applied Physics **6**(3): 289-304.

[11]. Whitehouse, David John, and J. F. Archard. "The properties of random surfaces of significance in their contact." Proceedings of the Royal Society of London A: Mathematical, Physical and Engineering Sciences. Vol. 316. No. 1524. The Royal Society, 1970.

[12]. Bush, A. W., R. D. Gibson, and G. P. Keogh. "Strongly anisotropic rough surfaces." Journal of Lubrication Technology 101.1 (1979): 15-20.

[13]. Polycarpou, Andreas A., and Izhak Etsion. "Analytical approximations in modeling contacting rough surfaces." ASME J. Tribol 121.2 (1999): 234-239.

[14]. McCool, John I. "Non-Gaussian effects in microcontact." International Journal of Machine Tools and Manufacture 32.1-2 (1992): 115-123.

[15]. Chilamakuri, S. K., and Bharat Bhushan. "Contact analysis of non-Gaussian random surfaces." Proceedings of the Institution of Mechanical Engineers, Part J: Journal of Engineering Tribology 212.1 (1998): 19-32.

[16]. Kim, T. W., B. Bhushan, et al. (2006). "The contact behavior of elastic/plastic non-Gaussian rough surfaces." Tribology Letters **22**(1): 1-13.

[17]. Nayak, P. R. (1973). "Random Process Model of Rough Surfaces in Plastic Contact." Wear **26**(3): 305-333.

[18]. Nayak P. Ranganath. "Random process model of rough surfaces." ASME, 1971.

[19]. Francis, H. A. (1977). "Application of Spherical Indentation Mechanics to Reversible and Irreversible Contact between Rough Surfaces." Wear **45**(2): 221-269.

[20]. Francis, H. A. (1976). "Phenomenological Analysis of Plastic Spherical Indentation." Journal of Engineering Materials and Technology-Transactions of the Asme **98**(3): 272-281.

[21]. Chang, W. R., I. Etsion, et al. (1987). "An Elastic-Plastic Model for the Contact of Rough Surfaces." Journal of Tribology-Transactions of the Asme **109**(2): 257-263.

[22]. Zhao, Y. W. and L. Chang (2001). "A model of asperity interactions in elastic-plastic contact of rough surfaces." Journal of Tribology-Transactions of the Asme **123**(4): 857-864.

[23]. Peng, W. and B. Bhushan (2002). "Sliding contact analysis of layered elastic/plastic solids with rough surfaces." Journal of Tribology-Transactions of the Asme **124**(1): 46-61.

[24]. Kogut, L. and I. Etsion (2003). "A finite element based elastic-plastic model for the contact of rough surfaces." Tribology Transactions **46**(3): 383-390.

[25]. Jackson, R.L. and I. Green, *A statistical model of elasto-plastic asperity contact between rough surfaces.* Tribology International, 2006. **39**(9): p. 906-914.

[26]. Jackson, R.L. and I. Green, *A Finite Element Study of Elasto-Plastic Hemispherical Contact Against a Rigid Flat.* Journal of Tribology, 2005. **127**(2): p. 343-354.

[27]. Archard, J. F. (1957). "Elastic deformation and the laws of friction." Proceedings of the Royal Society of London. Series A. Mathematical and Physical Sciences **243**(1233): 190-205.

[28]. Majumdar, A. and B. Bhushan (1991). "Fractal Model of Elastic-Plastic Contact between Rough Surfaces." Journal of Tribology-Transactions of the Asme **113**(1): 1-11.

[29]. Ciavarella, M., G. Demelio, et al. (2000). "Linear elastic contact of the Weierstrass profile." Proceedings of the Royal Society a-Mathematical Physical and Engineering Sciences **456**(1994): 387-405.

[30]. Westergaard, H. "Bearing Pressures and Cracks." Journal of applied mechanics 18 (1939).

[31]. Gao, Y. F., A. F. Bower, et al. (2006). "The behavior of an elastic-perfectly plastic sinusoidal surface under contact loading." Wear **261**(2): 145-154.

[32]. Jackson, R. L. and J. L. Streator (2006). "A multi-scale model for contact between rough surfaces." Wear **261**(11-12): 1337-1347.

[33]. Johnson, K. L., J. A. Greenwood, et al. (1985). "The contact of elastic regular wavy surfaces." International Journal of Mechanical Sciences **27**(6): 383-396.

[34]. Wilson, W. E., S. V. Angadi, et al. (2010). "Surface separation and contact resistance considering sinusoidal elastic-plastic multi-scale rough surface contact." Wear **268**(1-2): 190-201.

[35]. Krithivasan, V. and R. L. Jackson (2007). "An analysis of three-dimensional elasto-plastic sinusoidal contact." Tribology Letters **27**(1): 31-43.

[36]. Jackson, R. L., V. Krithivasan, et al. (2008). "The pressure to cause complete contact between elastic—plastic sinusoidal surfaces." Proceedings of the Institution of Mechanical Engineers, Part J: Journal of Engineering Tribology **222**(7): 857-863.

[37]. Manners, W. (2008). "Plastic deformation of a sinusoidal surface." Wear **264**(1): 60-68.

[38]. Ghaednia, H., Wang, X.,Saha, S., Jackson, R.L., Xu, Y., Sharma, A., *A Review of Elastic-Plastic Contact Mechanics.* Applied mechanics reviews, 2017: p. in print.

[39]. Rostami, A. and J. L. Streator (2015). "Study of liquid-mediated adhesion between 3D rough surfaces: A spectral approach." Tribology International **84**: 36-47.

[40]. Komvopoulos, K. and D. H. Choi (1992). "Elastic Finite Element Analysis of Multi-Asperity Contacts." Journal of Tribology **114**(4): 823-831.

[41]. Tian, X. F. and B. Bhushan (1996). "A numerical three-dimensional model for the contact of rough surfaces by variational principle." Journal of Tribology-Transactions of the Asme **118**(1): 33-42.

[42]. Hyun, S., et al (2004). "Finite-element analysis of contact between elastic self-affine surfaces." Physical Review E **70**(2): 026117.

[43]. Pei, L., S. Hyun, et al. (2005). "Finite element modeling of elasto-plastic contact between rough surfaces." Journal of the Mechanics and Physics of Solids **53**(11): 2385-2409.

[44]. Pasaribu, H. R. and D. J. Schipper (2005). "Application of a deterministic contact model to analyze the contact of a rough surface against a flat layered surface." Journal of Tribology-Transactions of the Asme **127**(2): 451-455.

[45]. Megalingam, A., and M. M. Mayuram. "A FEM based multiple asperity deterministic contact model." ASME/STLE 2009 International Joint Tribology Conference. American Society of Mechanical Engineers, 2009.

[46]. Thompson, M. Kathryn. "Methods for generating rough surfaces in ANSYS." Proceedings of the 2006 International ANSYS Users Conference & Exhibition, Pittsburgh, PA. 2006.

[47]. Megalingam, A. and M. M. Mayuram (2014). "Effect of surface parameters on finite element method based deterministic Gaussian rough surface contact model." Proceedings of the Institution of Mechanical Engineers Part J-Journal of Engineering Tribology **228**(12): 1358-1373.

[48]. Song, H., E. Van der Giessen, et al. (2016). "Strain gradient plasticity analysis of elasto-plastic contact between rough surfaces." Journal of the Mechanics and Physics of Solids **96**: 18-28.

[49]. Liu, G., J. Zhu, et al. (2001). "Elasto-plastic contact of rough surfaces." Tribology Transactions 44(3): 437-443.

[50]. Jamari, J., M. B. de Rooij, et al. (2007). "Plastic Deterministic Contact of Rough Surfaces." Journal of Tribology **129**(4): 957-962.

[51]. Wang, Z. J., W. Z. Wang, et al. (2010). "A Numerical Elastic-Plastic Contact Model for Rough Surfaces." Tribology Transactions **53**(2): 224-238.

[52]. Jackson, R.L. and I. Green, *On the Modeling of Elastic Contact between Rough Surfaces.* Tribology Transactions, 2011. **54**(2): p. 300-314.

[53]. Yastrebov, V. A., J. Durand, et al. (2011). "Rough surface contact analysis by means of the Finite Element Method and of a new reduced model." Comptes Rendus Mecanique **339**(7-8): 473-490.

[54]. Y. Xu, "An Analysis of Elastic Rough Contact Models", Mechanical Engineering, Auburn University, Auburn, 2012.

[55]. Poulios, K. and P. Klit (2013). "Implementation and applications of a finite-element model for the contact between rough surfaces." Wear **303**(1-2): 1-8.

[56]. Brizmer, Victor, Yuri Kligerman, and Izhak Etsion (2007). "Elastic–plastic spherical contact under combined normal and tangential loading in full stick." Tribology Letters**25**(1): 61-70.

[57]. Brizmer, V., Y. Kligerman, and I. Etsion (2007). "A model for junction growth of a spherical contact under full stick condition." Journal of Tribology**129**(4): 783-790.

[58]. Zolotarevskiy, V., Y. Kligerman, and I. Etsion (2011). "The evolution of static friction for elastic-plastic spherical contact in pre-sliding." Journal of Tribology**133**(3): 034502.

Appendix A

Spectral Interpolation Method

```
clear all;
close all;
clc;

%
load R8G.txt;
Data=R8G;
X0=Data(:,1);
Y0=Data(:,2);
Z0=Data(:,3);
L_total=length(Z0);
NP=sqrt(L_total);
X=reshape(X0,NP,NP);
Y=reshape(Y0,NP,NP);
ZZ=reshape(Z0,NP,NP);

%2048
XX=X(:,1);
YY=Y(1,:);
X0=XX(1:1024);
Y0=YY(1:1024);
Z0=ZZ(1:1024,1:1024);

%32
X0=XX(1:32);
Y0=YY(1:32);
Z0=ZZ(1:32,1:32);

Interval_x=X0(2)-X0(1);
Interval_y=Y0(2)-Y0(1);

NP0=32;     % Number of points for the original data
NP1=62;     % Number of points after first interpolation
NP2=124;    % Number of points on each line after second interpolation


X0=(0:NP0-1)*(Interval_x/2^0);
Y0=(0:NP0-1)*(Interval_y/2^0);

X1=(0:NP1)*(Interval_x/2^1);
Y1=(0:NP1)*(Interval_y/2^1);

NP=32;
```

```
        a =   0.0001502;
        b =    -0.06012;
        c =    -0.06551;
        d =      -9.223;
        e =      -1.291;


        for i=1:NP
        for j=1:NP
        Zf(i,j)=(a*X0(i)+b)*(c*Y0(j)+d)+e;
         end
        end

Z2=Z0-Zf';
Zmean=mean(mean(Z2));
Z3=Z2-Zmean;
% ZZ1=[Z3,Z3(:,1);Z3(1,:),Z3(1,1)];
% ZZ2=reshape(ZZ1,33^2,1);

% Zmean=mean(mean(Z3));
Zm=max(max(Z3));
Zn=min(min(Z3));




% _____________________first interpolation (63*63)_____________________

ZZ3=fftshift(fft2(ifftshift(Z3)));

ZZ_new=zeros(64,64);
ZZ_new(17:48,17:48)=ZZ3;
Z_new=fftshift(ifft2(ifftshift(ZZ_new)));
Z_new1=4*real(Z_new);
Z_new2=Z_new1(1:63,1:63);
Z_new3=reshape(Z_new2,63^2,1);

% _____________________second interpolation (125*125)_____________________

ZZ3=fftshift(fft2(ifftshift(Z3)));

ZZ_new=zeros(128,128);
ZZ_new(49:80,49:80)=ZZ3;
Z_new=fftshift(ifft2(ifftshift(ZZ_new)));
Z_new1=16*real(Z_new);
Z_new2=Z_new1(1:125,1:125);
Z_new3=reshape(Z_new2,125^2,1);
```

Appendix B

ANSYS Simulation Code (125 by 125 case)

```
! ELASTIC-PERFECTLY PLASTIC ROUGH SURFACE CONTACT
! LENTH UNIT: MM

/FILNAME,4L_NP125_ep,1          !         Change name to Rs1

!*************************** Preprocessor ********************************

! -------------------------** ENTER PREPROCESSOR **-------------------------
/PREP7
!-------------------------Choose element type ---------------------------!
ET, 1, SOLID185         ! Solid 185 (8-node brick element)
ET, 2, TARGE170         ! Type 2 = 4-node target element
ET, 3, CONTA173         ! Type 3 = 8-node contact element
!-------------------------Set the element keyoptions ---------------------------!
KEYOPT,2,2,0            ! Boundary conditions for rigid target nodes: Specified by user.
KEYOPT,3,1,0            ! Degree of Freedom: UX,UY,UZ (default)
KEYOPT,3,2,0            ! Contact algorithm: AAugmented Lagrangian (default)
KEYOPT,3,4,2            ! Location of contact detection point: nomal to target surface
KEYOPT,3,5,3            ! CONF/ICONT automated adjustment: close gap with auto CNOF
KEYOPT,3,6,2            ! Contact stiffness variation: make a nomal refinement
KEYOPT,3,7,0            ! Element level time incrementation control: no control (default)
KEYOPT,3,8,0            ! Asymmetric contact selection: No action (default)
KEYOPT,3,9,1            ! Effect of initial penetration or gap: Exclude both
KEYOPT,3,10,2           ! Contact stiffness update: Each iteration
KEYOPT,3,11,0           ! Shell thickness effect: Exclude
KEYOPT,3,12,0           ! Behavior of contact surface: standard
KEYOPT,3,14,0           ! Behavior of fluid penetration load: various during iterations (default)
!-------------------------Set real constant ---------------------------!
R,1,0,0,20, 0.1,0,0     ! Set normal penalty stiffness factor and penalty stiffness 0.01
```

```
RMORE,,,, ,,
RMORE,,,, ,,
RMORE,,,, ,,
RMORE,,,,,,
!-------------------------set the material property ---------------------------!
MP, EX, 1, 200E3        ! Elastic modulus [N/mm^2]
MP, NUXY, 1, 0.3        ! Poisson's ratio
TB, BISO                ! Bilinear isotropic material model
TBDATA, 1, 1e3          ! Yield stress [N/mm^2]
TBDATA, 2, 1e2          ! Tangential modulus [N/mm^2]
! -------------------------* READ ROUGH SURFACE DATA *-------------------------
/INPUT, READ_SURFACE_DATA, TXT                  ! *VREAD HAS TO BE CALLED FROM EXTERNAL
FILE
DEL_X = L/(NP-1)
DEL_Y = L/(NP-1)
*SET, N_END, 5
*SET, NLAYERO, 5
*SET, H_BOTTOM, DEL_X*2**(NLAYERO)
*DIM, H_BSAE, ARRAY, NLAYERO
*DO, I, 1,NLAYERO
  H_BSAE(I) = DEL_X*2**(NLAYERO-I)
*ENDDO
!---------------------------------------Base set---------------------------------------
NLAYER_B=2*NLAYERO
*DIM, LDEPTH, ARRAY, NLAYER_B
LDEPTH(1)=H_BOTTOM
*DO, I, 2,NLAYER_B
  LDEPTH(I) = LDEPTH(I-1)+H_BSAE(NINT((I-1)/2))
*ENDDO
!---------------------------------------Surface set---------------------------------------
*SET, NLAYER_S, 5
*SET, H_SURFACE, 1.25e-3
*DIM, LDEPTH_T, ARRAY, NLAYER_S
*DO, I, 1,NLAYER_S
  LDEPTH_T(I) = LDEPTH(NLAYER_B)+I*(H_SURFACE/NLAYER_S)
*ENDDO
LDEPTH_TOP=LDEPTH_T(NLAYER_S)
```

```
!-----------------------------------CREATE VOLUME-----------------------------------------
*DO, I, 1, NLAYER_B
  *IF, I, EQ, 1, THEN
    BLC5, L/2, L/2, L, L, LDEPTH(I)
    WPOFFS, 0, 0, LDEPTH(I)
  *ELSE
    BLC5, L/2, L/2, L, L, LDEPTH(I) - LDEPTH(I-1)
    WPOFFS, 0, 0, LDEPTH(I) - LDEPTH(I-1)
  *ENDIF
*ENDDO

*DO, I, 1, NLAYER_S
  *IF, I, EQ, 1, THEN
    BLC5, L/2, L/2, L, L, H_SURFACE/NLAYER_S
    WPOFFS, 0, 0, H_SURFACE/NLAYER_S
  *ELSE
    BLC5, L/2, L/2, L, L, LDEPTH_T(I) - LDEPTH_T(I-1)
    WPOFFS, 0, 0, LDEPTH_T(I) - LDEPTH_T(I-1)
  *ENDIF
*ENDDO
VGLUE, ALL                              ! GLUE VOLUMES
NUMCMP, VOLU                            ! RENUMBER THE VOLUME ENTITIES
! -----------------------------------* MESH SUBSTRATE *-------------------------------
!-----------------------------------PRE MESH LAYER SURFACES-------------------------------
ASEL, S, LOC, Z, -DEL_X/10, DEL_X/10
LSLA, S
LESIZE, ALL,,,4
ALLSEL

ASEL, S, LOC, Z, LDEPTH(10)-DEL_X/10, LDEPTH(10)+DEL_X/10
LSLA, S
LESIZE, ALL,,,124
ALLSEL

*DO, I, 1, 9
  ASEL, S, LOC, Z, LDEPTH(I) - DEL_X/10, LDEPTH(I) + DEL_X/10
  LSLA, S
```

```
  LESIZE, ALL,,, 2**(NINT((I-1)/2))*(N_END-1)
  ALLSEL
*ENDDO
ALLSEL

*DO, I, 1, NLAYER_S
  ASEL, S, LOC, Z, LDEPTH_T(I) - DEL_X/10, LDEPTH_T(I) + DEL_X/10
  LSLA, S
  LESIZE, ALL,,, (NP-1)
  ALLSEL
*ENDDO
!------------------------------PRE MESH LINES ON SIDE SURFACES-------------------------------
*DO, I, 2, NLAYER_B
  KSEL, S, LOC, Z, LDEPTH(I-1)-DEL_X/10, LDEPTH(I) + DEL_X/10
  LSLK, S, 1
  LESIZE, ALL,,,1
  ALLSEL
*ENDDO
ALLSEL
*DO, I, 2, NLAYER_S
  KSEL, S, LOC, Z, LDEPTH_T(I-1)-DEL_X/10, LDEPTH_T(I) + DEL_X/10
  LSLK, S, 1
  LESIZE, ALL,,,1
  ALLSEL
*ENDDO
ALLSEL

KSEL, S, LOC, Z, LDEPTH(NLAYER_B)-DEL_X/10, LDEPTH_TOP + DEL_X/10
KSEL, A, LOC, Z, -DEL_X/10, LDEPTH(1) + DEL_X/10
LSLK, S, 1
LESIZE, ALL,,,1
ALLSEL
!---------------------------------------MESH-----------------------------------
TYPE, 1                                 ! SOLID 95
MAT, 1                                  ! LINEAR ELASTIC
MSHAPE, 0, 3D                           ! ELEMENT SHAPE: 3D BRICK
MSHKEY,1                                ! MAPPED MESHING
```

```
VSEL,S,VOLU, ,NLAYER_B+1,NLAYER_B+NLAYER_S
 VMESH, ALL

MOPT, PYRA, ON                          ! TURN ON PYRAMID ELEMENT TRASITION STRATEGY
MSHAPE, 1, 3D                           ! ELEMENT SHAPE: 3D TETRAHEDRAL
MSHKEY,0                                ! FREE MESHING

VSEL,S,VOLU, ,1,NLAYER_B
VMESH, ALL                              ! MESHING LAYER 3, 2, 1
! -------------------------* MODEL RIGID FLAT *-------------------------
ASEL, U, AREA, , ALL
ESEL, U, ELEM, , ALL
NSEL, U, NODE, , ALL

*SET,DEL_L , 0
K, 1001, -L/8, -L/8, LDEPTH_TOP+ DEL-DEL_L
K, 1002, -L/8, L+L/8, LDEPTH_TOP + DEL-DEL_L
K, 1003, L+L/8, L+L/8, LDEPTH_TOP + DEL-DEL_L
K, 1004, L+L/8, -L/8, LDEPTH_TOP + DEL-DEL_L

A, 1001, 1004, 1003, 1002
CM, RIGID_FLAT, AREA
WPOFFS, 0, 0, DEL-DEL_L
ALLSEL
! -------------------------* IDENTIFY CONTACT PAIR *-------------------------
ASEL,S,AREA, ,RIGID_FLAT
LSLA
LESIZE, ALL,,, 1
ASEL,S,AREA, ,RIGID_FLAT
TYPE, 2
AMESH, ALL
ESURF, ALL, REVERSE
! ------------------------------* Define Pilot node *-------------------------------!
TSHAP, PILO
N, 1E8 ,-L/32, -L/32, LDEPTH_TOP+ DEL-DEL_L
E, 1E8
```

```
NSEL, S , , , 1E8
CM, PILOT, NODE
ALLSEL
! --------------------------------* meshing contact *--------------------------------!
NSEL, S, LOC, Z, LDEPTH_TOP - DEL_X/10, LDEPTH_TOP + DEL_X/10
TYPE, 3
MAT, 1
ESLN, S, 0
ESURF
ALLSEL

! ----------**********  Moving nodes  **********----------!
/NUMBER,-1
/PNUM,ELEM,0
!-----------------------------------DEFINE COMPONENTS------------------------------
NSEL, S, LOC, Z, LDEPTH_T(1) - DEL_X/10, LDEPTH_T(1) + DEL_X/10
CM, SURFACE_TOP1, NODE
ALLSEL

NSEL, S, LOC, Z, LDEPTH_T(2) - DEL_X/10, LDEPTH_T(2) + DEL_X/10
CM, SURFACE_TOP2, NODE
ALLSEL

NSEL, S, LOC, Z, LDEPTH_T(3) - DEL_X/10, LDEPTH_T(3) + DEL_X/10
CM, SURFACE_TOP3, NODE
ALLSEL

NSEL, S, LOC, Z, LDEPTH_T(4) - DEL_X/10, LDEPTH_T(4) + DEL_X/10
CM, SURFACE_TOP4, NODE
ALLSEL

NSEL, S, LOC, Z, LDEPTH_T(5) - DEL_X/10, LDEPTH_T(5) + DEL_X/10
CM, SURFACE_TOP5, NODE
ALLSEL

*SET,NUM_NODE,NP*NP
*DIM, NODE_LIST_A1,ARRAY,NUM_NODE
```

```
*DIM, NODE_LIST_A2,ARRAY,NUM_NODE
*DIM, NODE_LIST_A3,ARRAY,NUM_NODE
*DIM, NODE_LIST_A4,ARRAY,NUM_NODE
*DIM, NODE_LIST_A5,ARRAY,NUM_NODE

*DIM, NODE_LOCX_A1,ARRAY,NUM_NODE
*DIM, NODE_LOCX_A2,ARRAY,NUM_NODE
*DIM, NODE_LOCX_A3,ARRAY,NUM_NODE
*DIM, NODE_LOCX_A4,ARRAY,NUM_NODE
*DIM, NODE_LOCX_A5,ARRAY,NUM_NODE

*DIM, NODE_LOCY_A1,ARRAY,NUM_NODE
*DIM, NODE_LOCY_A2,ARRAY,NUM_NODE
*DIM, NODE_LOCY_A3,ARRAY,NUM_NODE
*DIM, NODE_LOCY_A4,ARRAY,NUM_NODE
*DIM, NODE_LOCY_A5,ARRAY,NUM_NODE

*DIM, NODE_LOCZ_A1,ARRAY,NUM_NODE
*DIM, NODE_LOCZ_A2,ARRAY,NUM_NODE
*DIM, NODE_LOCZ_A3,ARRAY,NUM_NODE
*DIM, NODE_LOCZ_A4,ARRAY,NUM_NODE
*DIM, NODE_LOCZ_A5,ARRAY,NUM_NODE

*DIM, NODE_ROUGHNESS_A1,ARRAY,NUM_NODE
*DIM, NODE_ROUGHNESS_A2,ARRAY,NUM_NODE
*DIM, NODE_ROUGHNESS_A3,ARRAY,NUM_NODE
*DIM, NODE_ROUGHNESS_A4,ARRAY,NUM_NODE
*DIM, NODE_ROUGHNESS_A5,ARRAY,NUM_NODE
!------------------- MOVINGN NODES ON THE SURFACE 5-------------------------
ESEL, S, TYPE, , 3
NSLE, S, ALL
*VGET,NODE_LIST_A5,NODE, ,NLIST
MODMSH, DETACH
SHPP,OFF
CONT_ELEM_LOC
*DO, I, 1, NUM_NODE
   *GET, NODE_LOCX_A5(I), NODE, NODE_LIST_A5(I), LOC, X
```

```
   *GET, NODE_LOCY_A5(I), NODE, NODE_LIST_A5(I), LOC, Y
   *GET, NODE_LOCZ_A5(I), NODE, NODE_LIST_A5(I), LOC, Z
   *SET,X5,NODE_LOCX_A5(I)
   *SET,Y5,NODE_LOCY_A5(I)
   *SET,Z5,NODE_LOCZ_A5(I)
   INDEX_X5 = X5/DEL_X+1
   INDEX_Y5 = Y5/DEL_Y+1
   *SET, NODE_ROUGHNESS_A5(I),ZZ(INDEX_X5, INDEX_Y5)
   NMODIF,NODE_LIST_A5(I),X5,Y5,Z5+(5/5)*NODE_ROUGHNESS_A5(I)
*ENDDO
!------------------- MOVINGN NODES ON THE SURFACE 4-------------------------
ALLSEL
NSEL, S, NODE,  , SURFACE_TOP4
*VGET,NODE_LIST_A4,NODE, ,NLIST
*DO, I, 1, NUM_NODE
   *GET, NODE_LOCX_A4(I), NODE, NODE_LIST_A4(I), LOC, X
   *GET, NODE_LOCY_A4(I), NODE, NODE_LIST_A4(I), LOC, Y
   *GET, NODE_LOCZ_A4(I), NODE, NODE_LIST_A4(I), LOC, Z
   *SET,X4,NODE_LOCX_A4(I)
   *SET,Y4,NODE_LOCY_A4(I)
   *SET,Z4,NODE_LOCZ_A4(I)
   INDEX_X4 = X4/DEL_X+1
   INDEX_Y4 = Y4/DEL_Y+1
   *SET, NODE_ROUGHNESS_A4(I),ZZ(INDEX_X4, INDEX_Y4)
   NMODIF,NODE_LIST_A4(I),X4,Y4,Z4+(4/5)*NODE_ROUGHNESS_A4(I)
*ENDDO
!------------------- MOVINGN NODES ON THE SURFACE 3-------------------------
ALLSEL
NSEL, S, NODE,  , SURFACE_TOP3
*VGET,NODE_LIST_A3,NODE, ,NLIST
*DO, I, 1, NUM_NODE
   *GET, NODE_LOCX_A3(I), NODE, NODE_LIST_A3(I), LOC, X
   *GET, NODE_LOCY_A3(I), NODE, NODE_LIST_A3(I), LOC, Y
   *GET, NODE_LOCZ_A3(I), NODE, NODE_LIST_A3(I), LOC, Z
   *SET,X3,NODE_LOCX_A3(I)
   *SET,Y3,NODE_LOCY_A3(I)
   *SET,Z3,NODE_LOCZ_A3(I)
```

```
   INDEX_X3 = X3/DEL_X+1
   INDEX_Y3 = Y3/DEL_Y+1
   *SET, NODE_ROUGHNESS_A3(I),ZZ(INDEX_X3, INDEX_Y3)
   NMODIF,NODE_LIST_A3(I),X3,Y3,Z3+(3/5)*NODE_ROUGHNESS_A3(I)

*ENDDO
!------------------- MOVINGN NODES ON THE SURFACE 2------------------------
ALLSEL
NSEL, S, NODE,  , SURFACE_TOP2
*VGET,NODE_LIST_A2,NODE, ,NLIST
*DO, I, 1, NUM_NODE
   *GET, NODE_LOCX_A2(I), NODE, NODE_LIST_A2(I), LOC, X
   *GET, NODE_LOCY_A2(I), NODE, NODE_LIST_A2(I), LOC, Y
   *GET, NODE_LOCZ_A2(I), NODE, NODE_LIST_A2(I), LOC, Z
   *SET,X2,NODE_LOCX_A2(I)
   *SET,Y2,NODE_LOCY_A2(I)
   *SET,Z2,NODE_LOCZ_A2(I)
   INDEX_X2 = X2/DEL_X+1
   INDEX_Y2 = Y2/DEL_Y+1
   *SET, NODE_ROUGHNESS_A2(I),ZZ(INDEX_X2, INDEX_Y2)
   NMODIF,NODE_LIST_A2(I),X2,Y2,Z2+(2/5)*NODE_ROUGHNESS_A2(I)
*ENDDO
!------------------- MOVINGN NODES ON THE SURFACE 1------------------------
ALLSEL
NSEL, S, NODE,  , SURFACE_TOP1
*VGET,NODE_LIST_A1,NODE, ,NLIST
*DO, I, 1, NUM_NODE
   *GET, NODE_LOCX_A1(I), NODE, NODE_LIST_A1(I), LOC, X
   *GET, NODE_LOCY_A1(I), NODE, NODE_LIST_A1(I), LOC, Y
   *GET, NODE_LOCZ_A1(I), NODE, NODE_LIST_A1(I), LOC, Z
   *SET,X1,NODE_LOCX_A1(I)
   *SET,Y1,NODE_LOCY_A1(I)
   *SET,Z1,NODE_LOCZ_A1(I)
   INDEX_X1 = X1/DEL_X+1
   INDEX_Y1 = Y1/DEL_Y+1
   *SET, NODE_ROUGHNESS_A1(I),ZZ(INDEX_X1, INDEX_Y1)
   NMODIF,NODE_LIST_A1(I),X1,Y1,Z1+(1/5)*NODE_ROUGHNESS_A1(I)
```

```
*ENDDO
! --------------------------------* Create components *---------------------------------!
ALLSEL
ESEL, S, TYPE, , 3
CM, ROUGH_SURFAEC_ELEM, ELEM
ALLSEL

ESEL, S, TYPE, , 2
NSLE, S, ALL
CM, TARGE_SURFACE, NODE
ALLSEL

NSEL, S, LOC, Z, -DEL_X/10, DEL_X/10
CM, BOTTOM_SURFACE, NODE
ALLSEL

NSEL, S, LOC, Y, -DEL_X/10, DEL_X/10
CM, FRONT_SURFACE, NODE
ALLSEL

NSEL, S, LOC, Y, L-DEL_X/10, L+DEL_X/10
CM, BACK_SURFACE, NODE
ALLSEL

NSEL, S, LOC, X, -DEL_X/10, +DEL_X/10
CM, LEFT_SURFACE, NODE
ALLSEL

NSEL, S, LOC, X, L-DEL_X/10, L+DEL_X/10
CM, RIGHT_SURFACE, NODE
ALLSEL
! --------------------------------* redefine element number type two *---------------------------------!
*SET, NCONTN, NP*NP
*SET, NCONTE, (NP-1)*(NP-1)
*DIM, NODE_LIST,ARRAY,NCONTN
*DIM, ELEM_LIST,ARRAY,NCONTE
*DIM, NODE_LOCX,ARRAY,NCONTN
```

```
*DIM, NODE_LOCY,ARRAY,NCONTN
*DIM, NODE_LOCZ,ARRAY,NCONTN

ESEL, S, TYPE, , 3
NSLE, S, ALL
*VGET,NODE_LIST,NODE, ,NLIST
*DO, I, 1, NCONTN
   *GET, NODE_LOCX(I), NODE, NODE_LIST(I), LOC, X
   *GET, NODE_LOCY(I), NODE, NODE_LIST(I), LOC, Y
   *GET, NODE_LOCZ(I), NODE, NODE_LIST(I), LOC, Z
*ENDDO
ALLSEL

ESEL, S, TYPE, , 3
*VGET,ELEM_LIST,ELEM, ,ELIST
ALLSEL
! ------------------------* X, Z and Node Number at Front Section *------------------------------!
  ESEL, S, TYPE,,1
  NSLE, S, ALL
  NSEL, R, LOC, Y, -DEL_X/10, DEL_X/10
  *VGET, LIST_FRONT, NODE, , NLIST
  *GET, NUM_FRONT,NODE,  , COUNT

  *DIM, X_FRONT, ARRAY, NUM_FRONT
  *DIM, Z_FRONT, ARRAY, NUM_FRONT
  *DO, J, 1, NUM_FRONT

   *GET, CX1, NODE, LIST_FRONT(J), LOC, X
   *SET, X_FRONT(J), CX1
   *GET, CZ1, NODE, LIST_FRONT(J), LOC, Z
   *SET, Z_FRONT(J), CZ1
  *ENDDO
ALLSEL

SAVE,'Moving','db'

! -------------------------------* Boundary conditions *--------------------------------!
```

```
/SOL
!Step 1. bottom surface
NSEL, S, NODE, , BOTTOM_SURFACE
D, ALL, ALL, 0
ALLSEL

! Step 2. Two side surfaces
NSEL, S, NODE, , LEFT_SURFACE
NSEL, A, NODE, , RIGHT_SURFACE
D, ALL, UX, 0
ALLSEL

! Step3 Front side and back surfaces
NSEL, S, NODE,  , FRONT_SURFACE
NSEL, A, NODE,  , BACK_SURFACE
D, ALL, UY, 0
ALLSEL

SAVE,'Boundary','db'
! ------------------------------* Apply the normal force on the rigid flat *------------------------------!
/SOLU
! 1ST LOADING STEP
ANTYPE, 0
LUMPM, 0
NLGEOM, 1
KBC, 0
AUTOTS, 1
NSUBST,10000,50000,200
Time, 100
NEQIT, 100
RESCONTROL, ,ALL,LAST,200
OUTRES, ALL, ALL

D, PILOT, UX, 0
D, PILOT, ROTX, 0
D, PILOT, UY, 0
D, PILOT, ROTY, 0
```

```
D, PILOT, UZ, -1.6*DEL
D, PILOT, ROTZ, 0

CUTCONTROL,PLSLIMIT,0.5
CNVTOL, F, , 0.005, 2, 0.0001                    ‘
CNCHECK,AUTO
SOLVE
SAVE

!*****************************Post Processor**********************************
/POST1
SET, 1
*GET, NSUBSTEP1, ACTIVE, 0, SOLU, NCMSS
*DIM, CONPRESS, ARRAY, NSUBSTEP1*NCONTE
*DIM, ESTATUS, ARRAY, NSUBSTEP1*NCONTE
*DIM, REACT_FZ_ARRAY, ARRAY, NSUBSTEP1
*DIM, UZP_ARRAY, ARRAY, NSUBSTEP1
*DIM, UZN_ARRAY, ARRAY, NSUBSTEP1*NCONTN
*DIM, VM_FRONT, ARRAY, NUM_FRONT*NSUBSTEP1
*DIM, PSN_FRONT, ARRAY, NUM_FRONT*NSUBSTEP1
*SET, REACT_FZ, 0
*SET, CONSTATUS, 0
*SET, U_ZP, 0
*SET, U_ZN, 0
*SET, PRESSURE, 0
*SET, VM1, 0
*SET, PSN1, 0

!-----------------------------------------------------Target---------------------------------------------------------
ALLSEL
*DO, I, 1, NSUBSTEP1
   SUBSET, 1, I
   *GET, U_ZP, NODE, 1E8, U, Z
   *SET, UZP_ARRAY(I), U_ZP
*ENDDO
!-------------------------------------------------Contact------------------------------------------------------
ALLSEL
```

```
ESEL, S, TYPE, , 3
NSLE, S, ALL

*DO, I, 1, NSUBSTEP1
   SUBSET, 1, I
    ETABLE, CONPRES, CONT, PRES
    ETABLE, CONSTAT, CONT, STAT

  *DO, II, 1, NCONTE
   *GET, PRESSURE, ETAB, 1, ELEM, ELEM_LIST(II)
   *SET, CONPRESS((I-1)*NCONTE + II) , PRESSURE
   *GET, CONSTATUS, ETAB, 2, ELEM, ELEM_LIST(II)
   *SET,ESTATUS((I-1)*NCONTE + II) , CONSTATUS
  *ENDDO

    FSUM, RSYS, CONT
    *GET, REACT_FZ, FSUM, 0, ITEM, FZ
    REACT_FZ = -REACT_FZ
   *SET, REACT_FZ_ARRAY(I), REACT_FZ
*ENDDO

*DO, I, 1, NSUBSTEP1
   SUBSET, 1, I
  *DO, II, 1, NCONTN
   *GET, U_ZN, NODE, NODE_LIST(II), U, Z
   *SET,UZN_ARRAY((I-1)*NCONTN + II) , U_ZN
  *ENDDO
*ENDDO

!-------------------------------------------------Solid-----------------------------------------------
ALLSEL
ESEL, S, TYPE, , 1
NSLE, S, ALL

*DO, I, 1, NSUBSTEP1
   SUBSET, 1, I
  *DO, J, 1, NUM_FRONT
```

```
    *SET, III, (I-1)*NUM_FRONT + J
     *GET, VM1, NODE, LIST_FRONT(J), S, EQV
    *SET, VM_FRONT(III), VM1
   *ENDDO
*ENDDO

*DO, I, 1, NSUBSTEP1
    SUBSET, 1, I
   *DO, J, 1, NUM_FRONT
    *SET, III, (I-1)*NUM_FRONT + J

     *GET, PSN1, NODE, LIST_FRONT(J), EPPL, EQV
    *SET, PSN_FRONT(III), PSN1
   *ENDDO
*ENDDO
/INPUT, WRITE_RESULTS, txt
```